Eurographics Workshop on Visual Computing for Biology and Medicine (2022)
M. Krone, T. W. Kuhlen, R. G. Raidou, and B. Sommer (Editors)

Supplementary Material: Structured Analysis of All Ensembles

In the supplementary material, we present the results of the tissue property analysis using TPAT and all generated dataset ensembles with the described evaluation approach. For the evaluation in the ablation data plot, we mainly focus on the ablation volume size and the tumor ablation amount. Those measurements give the most information about the tissue property effects on the ablation area in the context of RF ablations. The DICE coefficient mainly correlates with the healthy tissue ablation which must be as small as possible in RF ablations. However, ensuring a complete ablation of the tumor and the safety margin around it is the first priority in RF ablations. Therefore, for this analysis, the DICE coefficient is not used. All data presented in this analysis is taken from TPAT. For the formulae and some of the figures in this section we use the following abbreviations in Table 1 to improve readability.

Abbreviation	Meaning
TP	tissue property
D	density
HC	heat capacity
TC	thermal conductivity
BPR	relative blood perfusion rate
abl_data	ablation data measurement
abl_vol	ablation volume size
t_abl	tumor ablation size

Table 1: *Abbreviations used in this section.*

For the evaluation of the ensemble data, we define two metrics, the first one being the Δ_{abl_data} value, presented in Section 4.3 of the main article. Its value for each ensemble can be calculated by subtracting the minimum ablation data value of the ensemble from the maximum value and dividing the result by the average. The ablation data measurement is either the ablation volume size (*abl_vol*) or the tumor ablation amount (*t_abl*). This metric intends to describe how much the inspected tissue property in an ensemble affects the chosen ablation data measurement. It gives a quick indication whether the tissue property values have an effect at all and can be used to compare the influence of the tissue properties between different datasets, like in ensemble B to D.

The second metric is the $\Phi^{tp}_{abl\_data}$ value which reflects the value of the *mean change in ablation data per tissue property unit* metric of TPAT, presented in Section 4.3 of the main article. It provides information about the impact of a tissue's property value on the chosen ablation data. This is used within the datasets to compare the influence of the three tissue types to one another and between the datasets of the ensembles to examine changes in these values due to different segmentations or secondary property changes. The units of the tissue properties used in the following are given in Table 2.

Property name	property unit
density	$1\ kg/m$
heat capacity	$1\ \frac{J}{C}$
thermal conductivity	$0.001\ \frac{W}{m \cdot K}$
relative blood perfusion rate	$0.0001\ \frac{ml}{s \cdot cm}$
electric conductivity	$0.01\ \frac{S}{m \cdot \Phi}$
electric permittivity	$10\ \frac{F}{m}$
water ratio	0.001%

Table 2: *The property units used for the mean change in ablation data metric.*

The supplementary material also includes tables of the tissue property values that were used as parameter values for the simulation to create the ensembles, see Tables 14 and 15.

1. Density

1.1. Ensemble A

With the lowest ablation volume size being 12843.3 mm³ and the highest being 12923.1 mm³ for the particular tissue image, the impact of the density on the ablation area is relatively low with a value span of only 79.8 mm³ and a resulting Δ_{abl_vol} value of 0.620 (see Table 3). In case of the tumor ablation amount this value span is even lower with only 2.95 mm³ (0.066 Δ_{t_abl}). This makes the density an almost negligible property even though it is one of the few properties that does affect the ablation area at all.

Apart from examining the minimum and maximum values for the ablation data, the $\Phi^{d}_{abl\_vol}$ and $\Phi^{d}_{t\_abl}$ values for each tissue type were inspected (see Table 4). The values for this measurement show that the blood vessels' density does not affect the ablation area at all. The surfaces of the ablation data plot in Figure 1 confirm these claims by showing no change in the surface volume on the vessel axis. In contrast, the liver and tumor density both affect the ablation volume size on a similar scale with a mean change per liver density

	Minimum	Maximum	Average	Max.-Min.	Δ
Ablation Volume	12843.3	12923.1	12863.7	79.80	0.621
Tumor Ablation	4454.69	4457.64	4455.66	2.95	0.066

Table 3: *Ablation data measurements of the density dataset of ensemble A.*

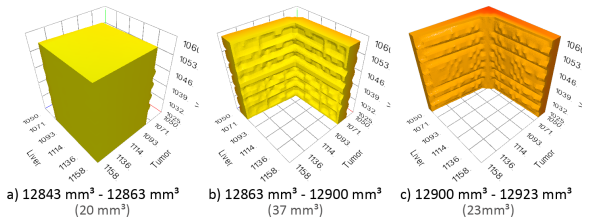

Figure 1: *Three surfaces for the ablation volume size.*

of -0.451 and a change per tumor density of -0.5641. Therefore is can be assumed that the highest ablation volume size is reached when those two values are the lowest and the lowest size is reached when the values are at their maximum.

Another important measurement to note here is the relatively high standard deviation of the $\Phi^d_{abl\_vol}$ value which is 1.1739 for the liver tissue and 1.1736 for the tumor tissue. It suggests a high variability of this value within the dataset. Further examination of the dataset in the ablation data plot discloses that the $\Phi^d_{abl\_vol}$ value decreases the further the liver and tumor density values are from their average values. This means a change in density of those tissue types has the most impact on the ablation volume when the density values are approximately between 1060 and 1080 kg/m^3. The surfaces also confirm the assumption that the highest ablation volume size is reached when those two values are the lowest and the lowest size is reached when the values are at their maximum.

Figure 2 shows five excerpts of the 3D view, with excerpt *a* showing the ablation volume for the average density values. The excerpts *b* to *d* use the average ablation volume as the intersect volume to demonstrate how the density of the liver and tumor tissue affects the ablation area. These volumes show that decreasing the liver or tumor density increases the volume of the ablation area around the tumor while decreasing it everywhere else. If, on the other hand, the density of the liver or the tumor takes on a high value, they differ in their behavior: While the high tumor density leads to a decrease in volume around the tumor, the high liver density leads to a decrease of the whole ablation area. Also, if the ablation volume is close to a blood vessel, the effects of a change in density that enlarges the volume are diminished. However, this mitigation only happens, when the ablation volume is right next to the blood vessel, with a distance below approximately 3mm (see Figure 3). More in-depth investigations on the ablation area have not been made due to the overall small change in volume.

1.2. Ensemble B

For ensemble B, in addition to the density property, the values of other tissue properties were also changed. These include the heat capacity, thermal conductivity and relative blood perfusion rate.

The blood vessel's heat capacity does not affect the Δ_{t_abl} values of the dataset at all, as shown in Figure 4. However, the heat capacity values of the liver and tumor tissue slightly affect the Δ_{abl_vol} of the dataset. Lower values for these tissues properties reduce the Δ_{abl_vol} value and therefore the impact those tissue properties have on the ablation volume size.

The Φ values of the liver and tumor tissue, that are displayed in Figure 5, exhibit a more significant change in value with different heat capacity values. When increasing the liver's heat capacity the $\Phi^d_{abl\_vol}$ and $\Phi^d_{t\_abl}$ values for the tumor show a continuous negative increase while the liver values reside at their average value except for the the highest sample at 3618 $\frac{J}{K}$ heat capacity where both Φ values almost reach zero. An increase in the tumor's heat capacity results in the same behavior, only in the respective other tissue type. Therefore, higher heat capacity values of a tissue lead to a slightly higher impact of the respective other tissue on the ablation area. The special case where a tissue's heat capacity is at their highest values results in an almost complete negation of the density's effect on the ablation volume for the respective tissue, as shown in Figure 6.

For the thermal conductivity as the second tissue property, high values for the liver or tumor tissue reduce the Δ_{abl_vol} and Δ_{t_abl} values by approximately 2/3 (see Figure 7). This suggests that higher than average thermal conductivity values of the liver or tumor tissue reduce the impact of the density on the ablation area.

Examination of the $\Phi^d_{abl\_vol}$ and $\Phi^d_{t\_vol}$ values in the graphs of Figure 8 confirms this claim. An increase in the liver's thermal conductivity almost completely nullifies the density's influence on the ablation volume and the tumor ablation amount. Figure 9 visualizes this effect for the liver tissue. In addition, the tumor's $\Phi^d_{abl\_vol}$ and $\Phi^d_{t\_vol}$ values also get reduced with higher liver thermal conductivity values. Another notable finding is, that the Φ values for the liver also go towards zero, when the liver's thermal conductivity is lower than average. Changing the tumor's thermal conductivity in a similar fashion results in an analogous behavior of the $\Phi^d_{abl\_vol}$ and $\Phi^d_{t\_vol}$ values. It has to be noted that the tumor's thermal conductivity is assumed to be up to 20% higher than the one of the liver, resulting in different looking graphs.

Just like for the heat capacity, the blood vessel's thermal conductivity has no effect on the ablation area.

For the relative blood perfusion rate we only examine the size of the ablation volume, as some of the configurations already completely cover the tumor. Also, only the liver and tumor tissue are examined, as the blood vessel's perfusion is not simulated. Increasing the blood perfusion values for either of the two tissue types decreases the Δ_{abl_vol} values as shown in Figure 10. Lower than average perfusion values lead to way higher Δ_{abl_vol} values of up to 0.708 for the liver and up to 0.938 for the tumor tissue. In con-

	Φ^d liver	Stdev	Φ^d vessel	Stdev	Φ^d tumor	Stdev
Ablation Volume	-0.4514	1.1739	0	0	-0.5641	1.1736
Tumor Ablation	-0.0133	0.0381	0	0	-0.0228	0.0378

Table 4: *The $\Phi^d_{abl\_vol}$ and $\Phi^d_{t\_abl}$ values of the dataset.*

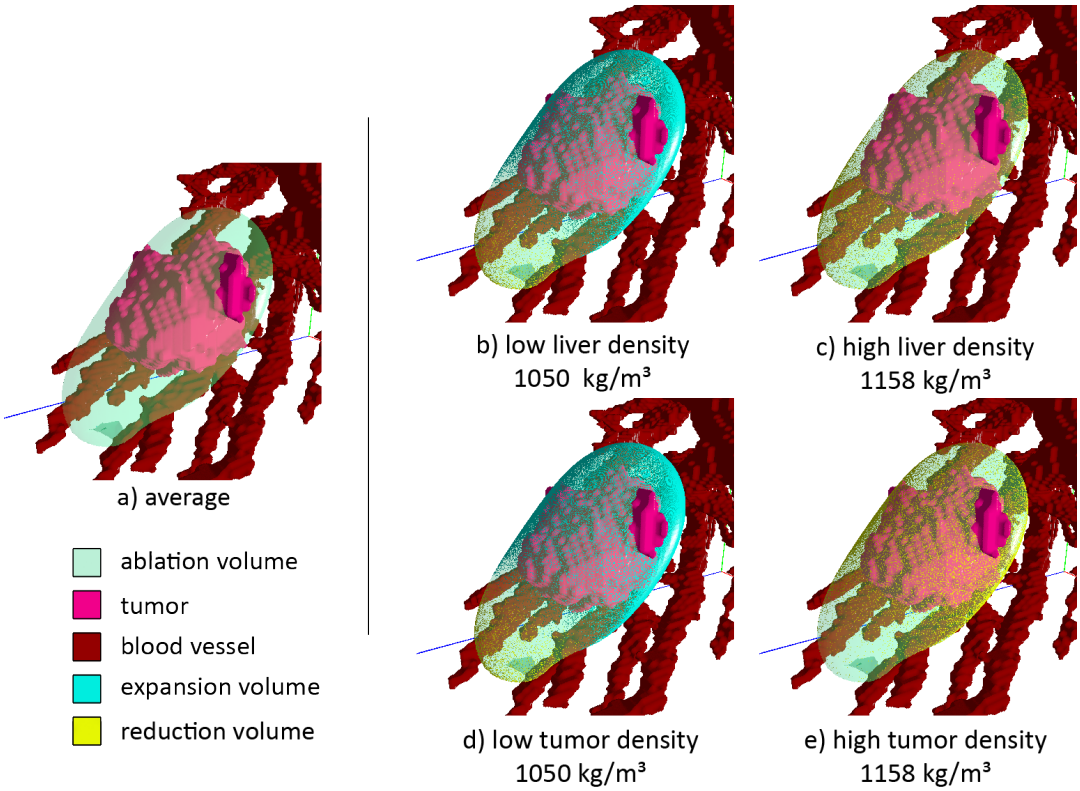

Figure 2: *Five excerpts of the 3D view visualizing the change in ablation volume due to different density values.*

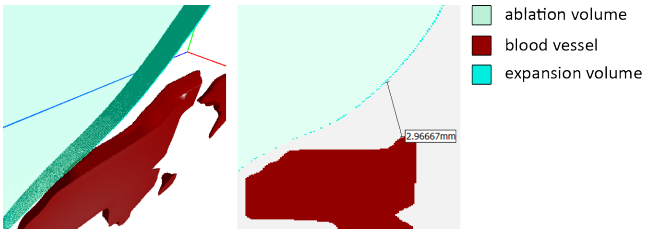

Figure 3: *Extracts of the 3D view and 2D view displaying the mitigation of the volume expansion due to blood vessel proximity.*

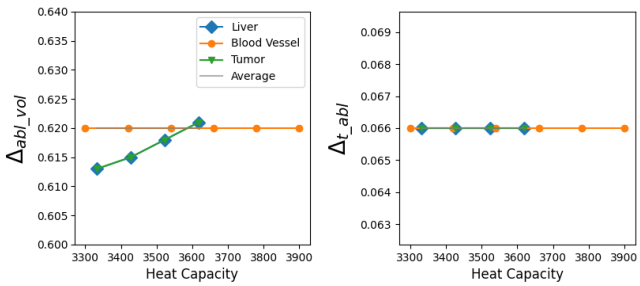

Figure 4: *The Δ_{abl_vol} and Δ_{t_abl} values for different heat capacity values.*

trast, increasing the blood perfusion ensures slightly lower Δ_{abl_vol} values with a minimum of 0.607 for the liver and 0.570 for the tumor tissue.

This suggests that a low blood perfusion heavily increases the density's effect on the ablation volume size while higher values slightly decrease it. The $\Phi^d_{abl\_vol}$ values in Figure 11 and the data in Table 5 support this claim.

1.3. Ensemble C

The ensemble C deals with different tumor sizes and their possible influence on the tissue properties. For the density, however, there is no change in its influence on the ablation data (see Figure 12). This is because the possible value ranges for the density of the tumor and

	low liver D $1050 kg/m^3$	high liver D $1158 kg/m^3$	low tumor D $1050 kg/m^3$	high tumor D $1158 kg/m^3$
average BPR values	0.292%	-0.098%	0.317%	-0.164%
low liver BPR $0.00652 \frac{ml}{s \cdot cm^3}$	0.221%	**-0.221%**	0.205%	-0.177%
high liver BPR $0.01967 \frac{ml}{s \cdot cm^3}$	0.311%	-0.068%	0.343%	-0.152%
low tumor BPR $0.0032 \frac{ml}{s \cdot cm^3}$	0.265%	-0.133%	0.354%	**-0.373%**
high tumor BPR $0.01967 \frac{ml}{s \cdot cm^3}$	0.327%	-0.097%	0.331%	-0.111%

Table 5: *The percentage increase in ablation volume size with low and high density and blood perfusion values for liver and tumor. The highlighted entries represent the biggest changes in ablation volume size compared to the average BPR values.*

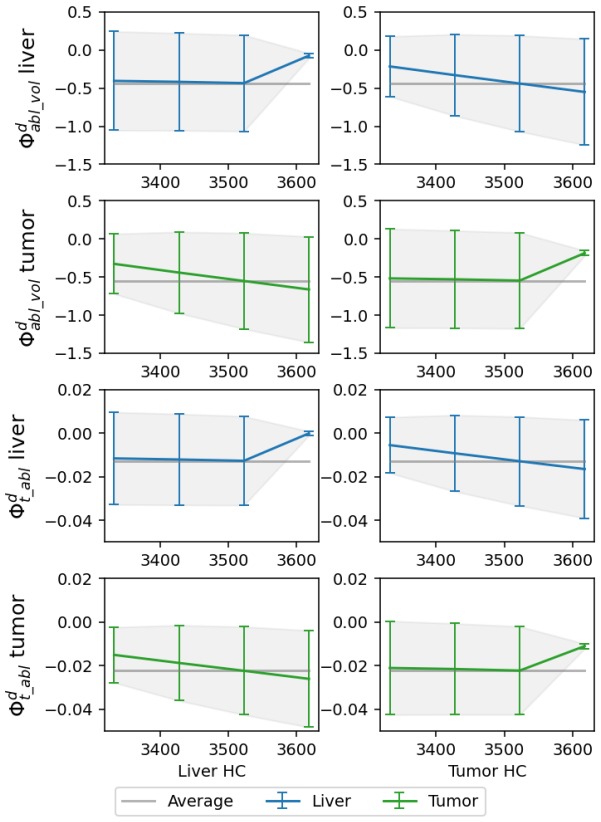

Figure 5: *The $\Phi^d_{abl\_vol}$ and $\Phi^d_{t\_abl}$ values and their standard deviation for the liver and tumor tissue with different heat capacity values.*

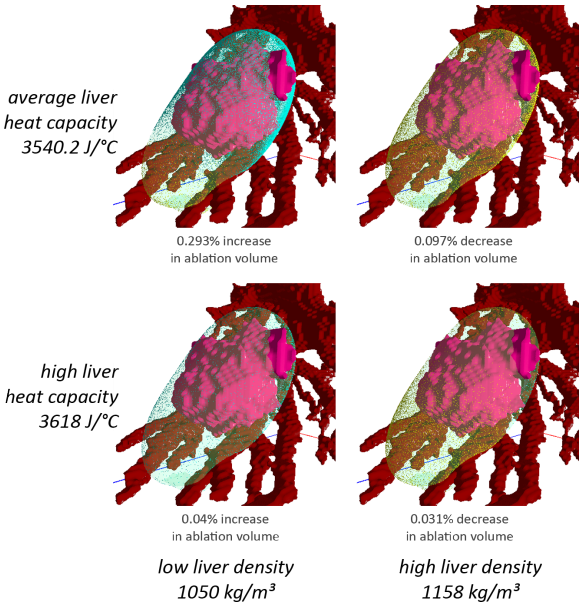

Figure 6: *The ablation volumes with different values for the density and heat capacity of the liver. The change in volume is in relation to the ablation volume of the average property values (liver HC = 3540.2 J/K, liver D = 1078.75 kg/m^3)*

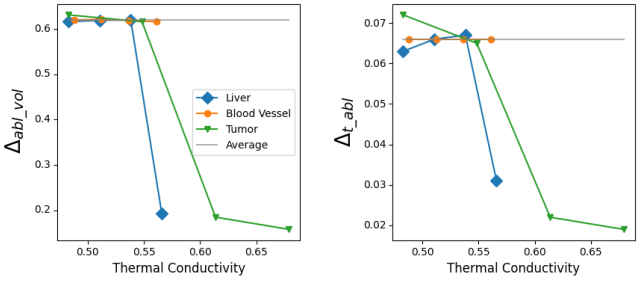

Figure 7: *The Δ_{abl_vol} and Δ_{t_abl} values for the liver and tumor tissue with different heat capacity values.*

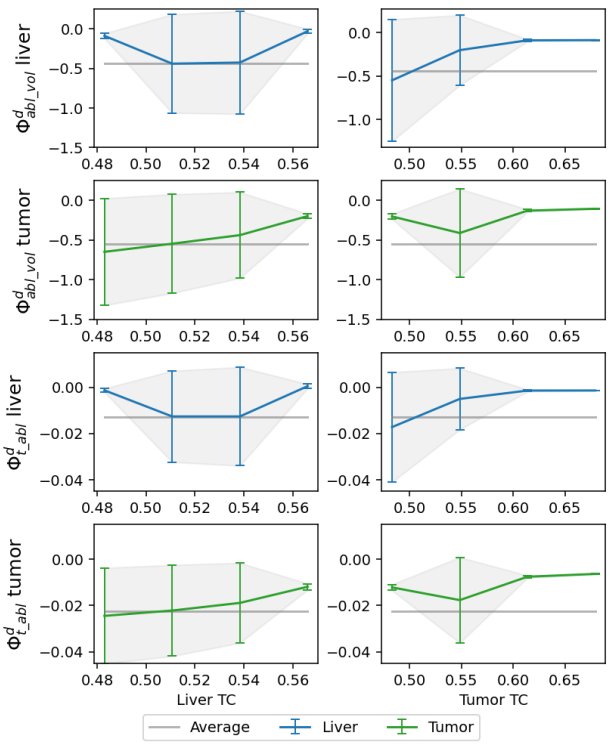

Figure 8: *The $\Phi^d_{abl\_vol}$ and $\Phi^d_{t\_abl}$ values and their standard deviation for the liver and tumor tissue with different thermal conductivity values.*

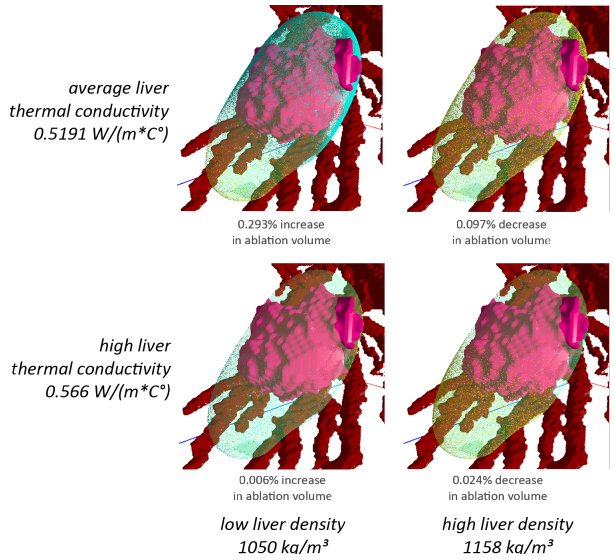

Figure 9: *The ablation volumes with different values for the density and thermal conductivity of the liver. The change in volume is in relation to the ablation volume of the average property values (liver TC = 0.5191 $\frac{W}{m \cdot K}$, liver D = 1078.75 kg/m^3)*

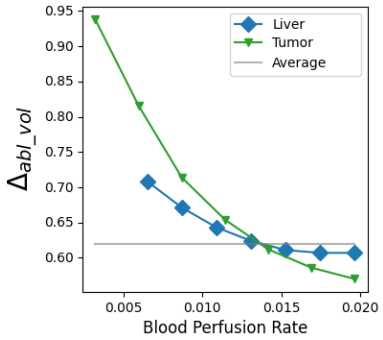

Figure 10: *The Δ_{abl_vol} values for the liver and tumor tissue with different blood perfusion rate values.*

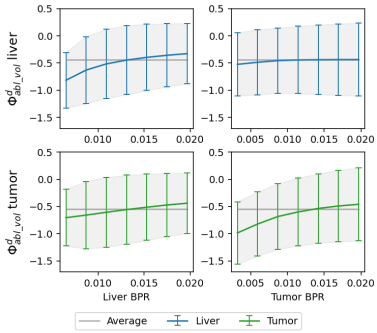

Figure 11: *The $\Phi^d_{abl\_vol}$ and $\Phi^d_{t\_abl}$ values and their standard deviation for the liver and tumor tissue with different blood perfusion rate values.*

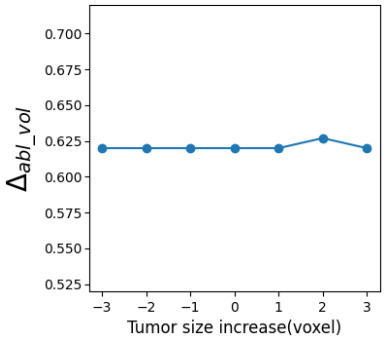

Figure 12: *The Δ_{abl_vol} values of the different tumor segmentations.*

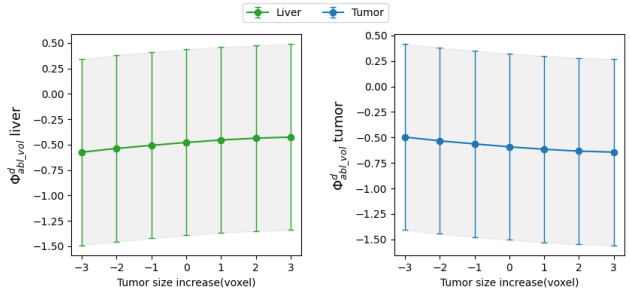

Figure 13: *The $\Phi^d_{abl\_vol}$ values and their standard deviation for the liver and tumor tissue with modified tumor segmentations.*

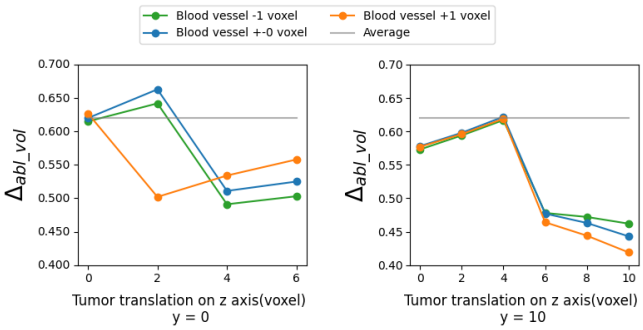

Figure 14: *The Δ_{abl_vol} and Δ_{t_abl} values for the liver and tumor tissue with different tumor segmentations and vessel sizes.*

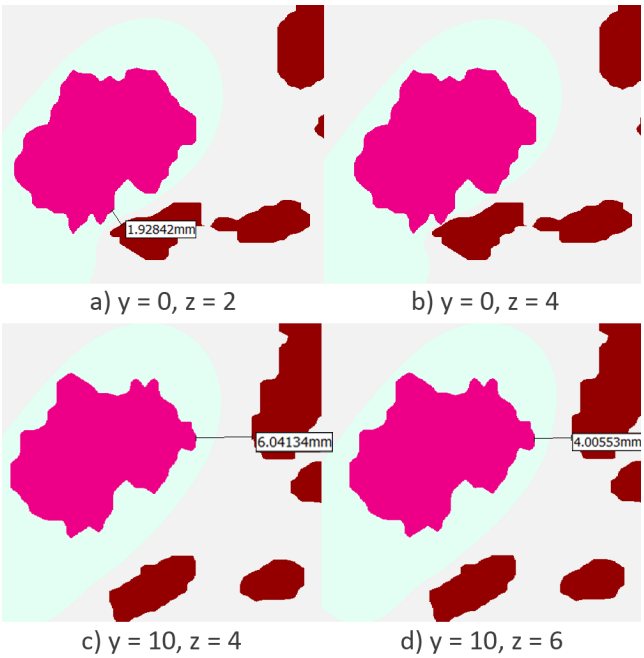

Figure 15: *Four extracts of the 2D view displaying the position of the tumor and the blood vessel cells.*

liver tissue are assumed to be the same. Therefore, a change in the tumor's size only changes the outcome of the RF ablation when the tumor's density differs from the density of the healthy liver tissue. Examination of the $\Phi^d_{abl\_vol}$ values in Figure 13 shows the negative decrease of the liver's $\Phi^d_{abl\_vol}$ value when the tumor gets bigger while the $\Phi^d_{abl\_vol}$ value of the tumor negatively increases. The tumor ablation amount is not considered for this ensemble as it is mainly influenced by the tumor size and therefore no conclusions can be drawn on the tissue properties. Viewing the ablation volume in the 3D view also shows no change in the previously observed behavior.

1.4. Ensemble D

For ensemble D the tumor position and vessel size were modified. Figure 14 displays the Δ_{abl_vol} values for the different tumor positions and vessel sizes. Here, the graphs are separated between the segmentations with a y-translation of 0 and 10 voxels.

Both segmentation types show a similar behavior when they are getting closer to the blood vessel tissue: At first, the Δ_{abl_vol} values increase slightly until they take a relatively large drop in value. Figure 15 displays four extracts of the 2D view that show the segmentations where this drop in value occurs. The reason for this behavior seem to be the proximity of the blood vessel cells. For the segmentations with a y-translation of 10 voxels, the blood vessels distance is much larger compared to the other segmentations, but these distant blood vessels are also bigger in size compared to the others which makes the size of the blood vessels also an important factor.

These findings suggest that the density has even less influence on the size of the ablation volume when the tumor's distance from the blood vessels falls below certain threshold. This is also dependent on the size of the blood vessels. In this case, the threshold lies between 4mm and 6mm when the blood vessels are relatively large like in extract *c* and *d* of Figure 15, whereas if the vessels are relatively small, as in extract *a* and *b*, the threshold's value is next to zero and the tumor directly touches the blood vessel.

The Δ_{t_abl} values of the ensemble only slightly change and do not show any pattern, thus they are not further inspected.

In case of the $\Phi^d_{abl\_vol}$ values, the same behavior as for the Δ_{abl_vol} values can be seen (see Figure 16). Here, the proximity of the blood vessel cells negatively decreases the $\Phi^d_{abl\_vol}$ value of the liver and tumor.

Examination of the ablation area in the 3D view shows that the influence of the liver and tumor density on the ablation volume differs between the segmentations with a y-translation value of 0 voxel and the ones with a y-traslation value of 10 voxel (see Figure 17). The ones with the a y-traslation value of 0 voxel all express an expansion of the volume towards the big blood vessel cluster they are moving to while the ones with a y-traslation value of 10 voxel also expand towards the blood vessels below them. Further differences between the ablation areas of the segmentations were not discovered since the overall change in ablation volume size due to different density values is really low.

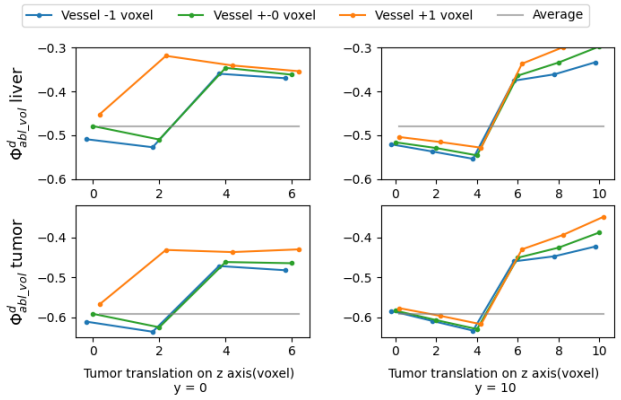

Figure 16: *The $\Phi^{d}_{abl\_vol}$ values for the liver and tumor tissue with different tumor segmentations and blood vessel sizes.*

2. Heat Capacity

2.1. Ensemble A

Moving on to the heat capacity property. The data in Table 6 shows that the heat capacity's influence on the ablation area is even smaller than the density's influence with a Δ_{abl_vol} value of 0.421 and a Δ_{t_abl} value of only 0.04.

The heat capacity of the liver and tumor both have an equal impact on the ablation volume size and the tumor ablation amount while the blood vessel's heat capacity has no impact at all (see Table 7). Furthermore, the $\Phi^{hc}_{abl\_vol}$ and $\Phi^{hc}_{t\_abl}$ values of the liver and tumor tissue have a high standard deviation which suggests a high fluctuation of these values within the dataset.

An examination of the surfaces in the ablation data plot confirms this assumption. Excerpts of the widget are shown in Figure 18. They display that the heat capacity's impact on the ablation volume size drastically decreases when the liver or tumor heat capacity are approximately above 3523 $\frac{J}{K}$ or when they are both below approximately 3477 $\frac{J}{K}$. They also disclose that the highest ablation volume size is reached when the liver and tumor heat capacity values are at their highest value. The surface for the tumor ablation amount exhibits the same pattern.

Figure 19 shows how the minimum and maximum values for the liver and tumor heat capacity affect the ablation volume. It can be seen that the volumetric changes are similar to the ones of the density: While low liver or low tumor heat capacity values expand the volume around the tumor towards the big blood vessels, the volume slightly decreases on the other end. In contrast, higher than average values result in a slight decrease of the whole ablation volume. Further investigations of the ablation volume did not yield new insights on this property's behavior since its overall impact is quite small.

2.2. Ensemble B

For ensemble B, the effects of the density, thermal conductivity and relative blood perfusion rate as the second property were investigated.

Starting with the density, as shown in Figure 20, an increase in the liver's or tumor's density only leads to a slight change in the Δ_{abl_vol} and Δ_{t_abl} values. However the $\Phi^{hc}_{abl\_vol}$ and $\Phi^{hc}_{t\_abl}$ values shown in Figure 21 of this dataset display a more significant change. An increase in the liver's or tumor's density leads to a continuous negative increase of the respective other tissue's $\Phi^{hc}_{abl\_vol}$ and $\Phi^{hc}_{t\_abl}$ values. Their own Φ values are mostly unaffected by these changes except for really high density values of approximately 1070 kg/m^3. Here, the $\Phi^{hc}_{abl\_vol}$ and $\Phi^{hc}_{t\_abl}$ of the corresponding tissue are almost completely nullified.

The excerpts of the 3D view in Figure 22 visualize the behavior of the liver's heat capacity. While higher than average heat capacity values have little to no influence on the ablation volume regardless of the density values, lower than average heat capacity values show a sharp decline when the density's value is high.

For the thermal conductivity a similar behavior like the one in the density dataset can be observed. High thermal conductivity values for either of the three tissue types lead to a sudden decrease of the respective Δ_{abl_vol} and Δ_{t_abl} values by about 90% (see Figure 23). The $\Phi^{hc}_{abl\_vol}$ and $\Phi^{hc}_{t\_abl}$ values in Figure 24 reveal why this sudden reduction of the Δ values occurs: When the thermal conductivity from either of the three tissue types is increased, the $\Phi^{hc}_{abl\_vol}$ and $\Phi^{hc}_{t\_abl}$ values for liver and tumor go against zero. Therefore their impact on the ablation area is almost nullified which explains the sudden drop in the Δ values.

Figure 25 illustrates the effect the thermal conductivity has on the heat capacity's impact on the ablation volume. The ablation volumes at the bottom almost show no volumetric changes and even slightly decrease in their size when the liver thermal conductivity is high. Increasing the vessel's or the tumor's thermal conductivity leads to very similar results.

Figure 26 shows that a higher than average blood perfusion rate leads to a similar increase in the Δ_{abl_vol} value of the liver and tumor while a lower perfusion leads to a decrease. The reduction in the liver's Δ_{abl_vol} values resembles an exponential reduction while the tumor's values seem to converge towards a Δ_{abl_vol} value of 0.38.

Although these Δ_{abl_vol} values suggest a high influence of the blood perfusion on the heat capacity, the $\Phi^{hc}_{abl\_vol}$ values in Figure 27 do not seem to differ a lot. Examining the absolute values for the ablation volume size, shown in Table 9, brings clarity. As previously stated, different blood perfusion values cause a strong change in the ablation volume size therefore the compared ablation volumes differ a lot. While the ablation volume is subject to a strong change in size, the difference between the maximum and minimum remains almost the same. This results in the observed Δ values. One reason for that could be that the heat capacity's effect on the ablation area is less affected by the size of the ablation volume. Another reason could be that the blood perfusion rate causes a reduction of the heat capacity's impact on the ablation volume. Due to the overall small impact the heat capacity has, no further investigation has been made on this. The 3D view also shows no significant changes compared to the previous results.

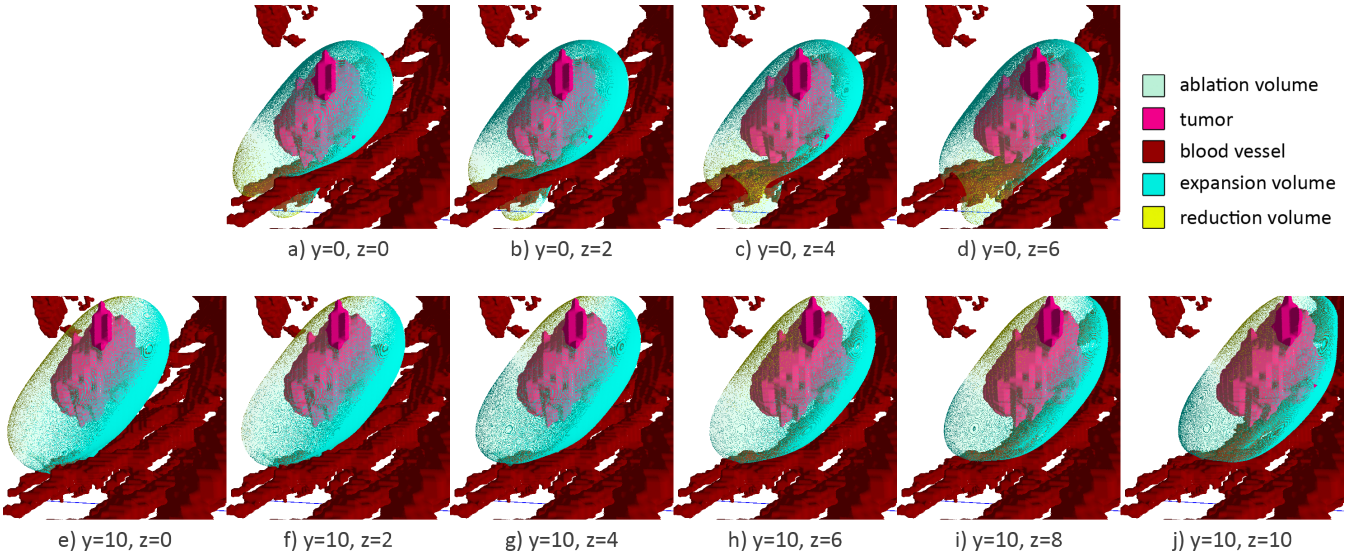

Figure 17: *Excerpts of the 3D view displaying the impact of negative liver density values on the different segmentations.*

	Minimum	Maximum	Average	Max.-Min.	Δ
Ablation Volume	12864.7	12915.9	12862.2	54.2	0.421
Tumor Ablation	4455.56	4457.33	4455.59	1.77	0.04

Table 6: *Ablation data measurements of the heat capacity dataset of ensemble A.*

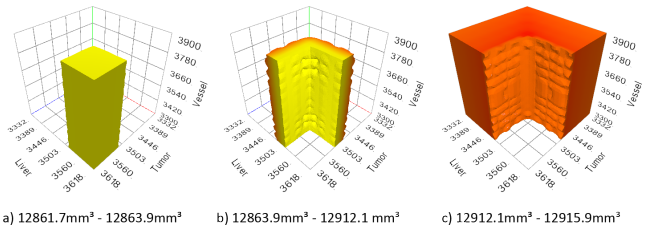

Figure 18: *Three surfaces of the ablation data plot displaying the coverage of the ablation volume size.*

2.3. Ensemble C

Just like for the density property, the Δ_{abl_vol} value of the heat capacity is also not affected by the size of the tumor. The $\Phi^{hc}_{abl\_vol}$ values for the liver and tumor also exhibit the same behavior as described in Section 1.3 of the supplemnentary material.

2.4. Ensemble D

Moving on to ensemble D of the heat capacity property, Figure 29 shows the Δ_{abl_vol} values of this ensemble. Here we also only present the Δ values for the ablation volume since the ones for the tumor ablation amount show no worthwhile information. The Δ_{abl_vol} values behave very similarly to those in ensemble D of the density property. After seemingly the same distance threshold from the blood vessels, most of them drop in their value. The Φ values also exhibit the same pattern like the ones of the density ensemble

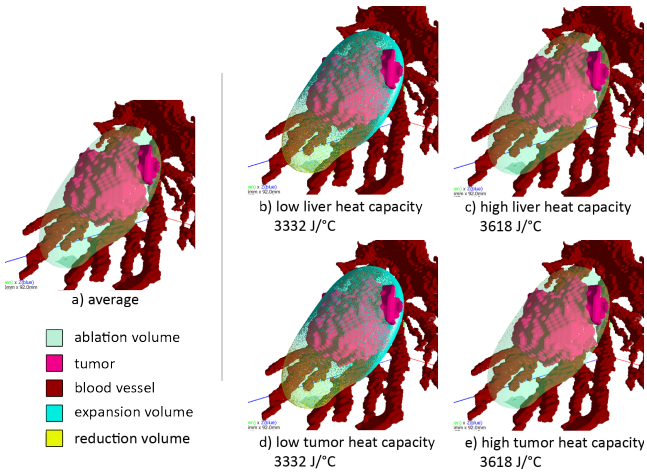

Figure 19: *Five excerpts of the 3D view visualizing the change in ablation volume due to different heat capacity values.*

although the actual value changes are way smaller than the ones of the density ensemble. The examination of the ablation area in the 3D view does not provide any new findings.

	Φ^{hc} liver	Stdev	Φ^{hc} vessel	Stdev	Φ^{hc} tumor	Stdev
Ablation Volume	-0.0760361	0.289213	0	0	-0.0755703	0.289299
Tumor Ablation	-0.00242774	0.00935062	0	0	-0.00258579	0.0093581

Table 7: *The $\Phi^{hc}_{abl\_vol}$ and $\Phi^{hc}_{t\_abl}$ values of the dataset.*

Liver BPR \ Abl. Vol.	Minimum	Maximum	Average	Max-Min
0.0065198	20100.5	20155	20104.4	54.50
0.00871183	16792.3	16848.9	16794.2	56.60
0.01090387	14575.2	14630.9	14576.4	55.70
0.0130959	12984.1	13038.3	12984.8	54.20
0.01528793	11786.3	11838.2	11786.8	51.90
0.01747997	10852.7	10901.8	10853.1	49.10
0.019672	10104.8	10151.8	10105.2	47.00

Table 8: *The absolute values for the ablation volume data with different liver blood perfusion values.*

Tumor BPR \ Abl. Vol.	Minimum	Maximum	Average	Max-Min
0.0032	14726	14781.9	14728.1	55.90
0.00594533	14161.6	14215.7	14163	54.10
0.00869	13646.8	13699.7	13647.7	52.90
0.011436	13168.8	13222.6	13169.5	53.80
0.01418	12720.9	12775.4	12721.4	54.50
0.01692	12292.3	12348	12292.7	55.70
0.019672	11884.1	11940.5	11884.5	56.40

Table 9: *The absolute values for the ablation volume data with different tumor blood perfusion values.*

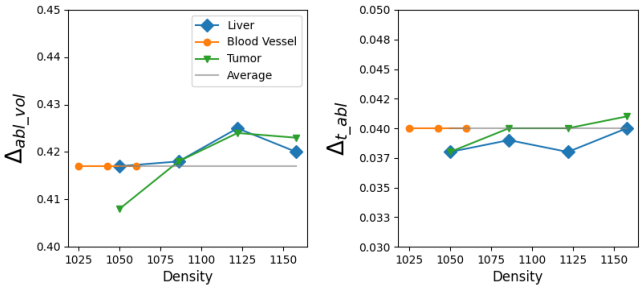

Figure 20: *The Δ_{abl_vol} and Δ_{t_abl} values of the dataset with different density values.*

3. Thermal Conductivity

3.1. Ensemble A

In ensemble A, only the thermal conductivity was changed and the default input tissue image was used. The influence of this property on the ablation volume is more than 4 times higher than the density's influence with a Δ_{abl_vol} value of 2.676 (see Table 10). Its influence on the tumor ablation in relation to the previous properties is even higher with a Δ_{t_abl} value of 0.891.

The size of the ablation area is mostly influenced by the thermal conductivity of the liver tissue with a $\Phi^{tc}_{abl\_vol}$ value of -2.694 (see Figure 11). The tumor and blood vessel thermal conductivity also affect the ablation volume but on a much smaller scale. In case of the tumor ablation amount, the liver's and the tumor's thermal conductivity both affect it on a similar scale but while liver thermal conductivity decreases the ablation amount, the tumor's thermal conductivity increases it. The blood vessel's value has almost no effect on the tumor ablation.

The Figures 31 and 32 show some surfaces of the ablation volume size and the tumor ablation amount that visualize the effect of the thermal conductivity values on the respective ablation data measurement. Further inspection shows that the highest ablation volume size is reached when the liver's and vessel's thermal conductivity is the lowest and the tumor's conductivity is the highest. The lowest volume size is reached when the opposite is the case. For the tumor ablation amount, the same pattern applies except for the vessel's thermal conductivity which has close to no impact on this ablation data measurement.

Using the 3D view of TPAT the ablation volumes for the minimum and maximum values of the three tissue types were investigated. Beginning with the liver's thermal conductivity. An increase of this tissue's thermal conductivity mainly reduces the volume where the tumor or the blood vessels are close to the edge of the ablation area as seen in Figure 33. Reducing it results in the opposite effect. Further investigation of the ablation volume reveals, that

	Minimum	Maximum	Average	Max.-Min.	Δ
Ablation Volume	12730.9	13076.3	12905	345.40	2.676
Tumor Ablation	4443.29	4482.99	4457.34	39.70	0.891

Table 10: *Ablation data measurements of the thermal conductivity dataset of ensemble A.*

	Φ^{tc} liver	Stdev	Φ^{tc} vessel	Stdev	Φ^{tc} tumor	Stdev
Ablation Volume	-2.69364	0.865949	-0.37052	0.615027	0.506056	0.590154
Tumor Ablation	-0.151284	0.0281706	0.00048534	0.0201293	0.138712	0.0319583

Table 11: *The $\Phi^{tc}_{abl\_vol}$ and $\Phi^{tc}_{t\_abl}$ values of the dataset.*

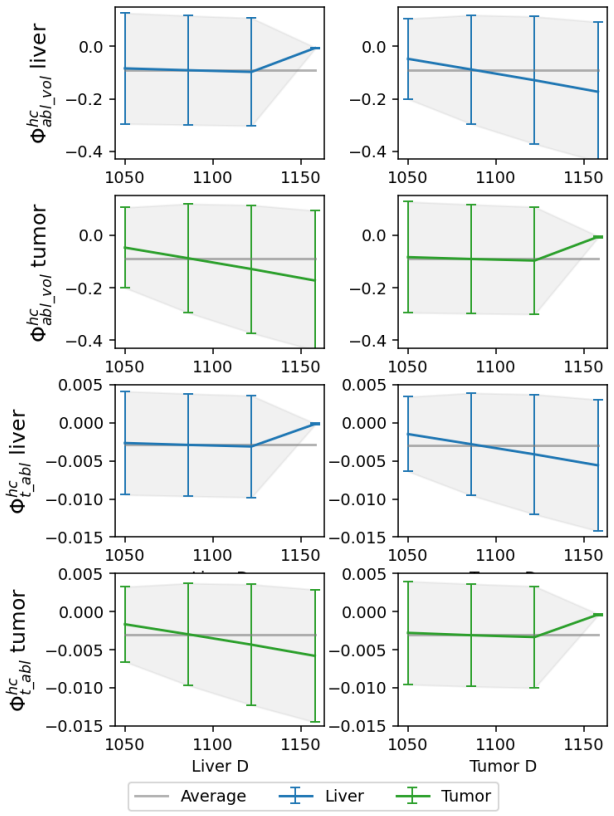

Figure 21: *The $\Phi^{hc}_{abl\_vol}$ and $\Phi^{hc}_{t\_abl}$ values and their standard deviation for the liver and tumor tissue with different density values.*

close blood vessels almost completely negate the thermal conductivity's impact on the ablation area. Figure 34 shows the part of the ablation volume which is up close to some blood vessels. There, the ablation volume seems almost completely unaffected by the liver's thermal conductivity values.

In case of the vessel's thermal conductivity, an increase leads to a reduction of the ablation volume near the blood vessel cells while slightly increasing the volume everywhere else. Lower than average values for this tissue result in an increase of the volume

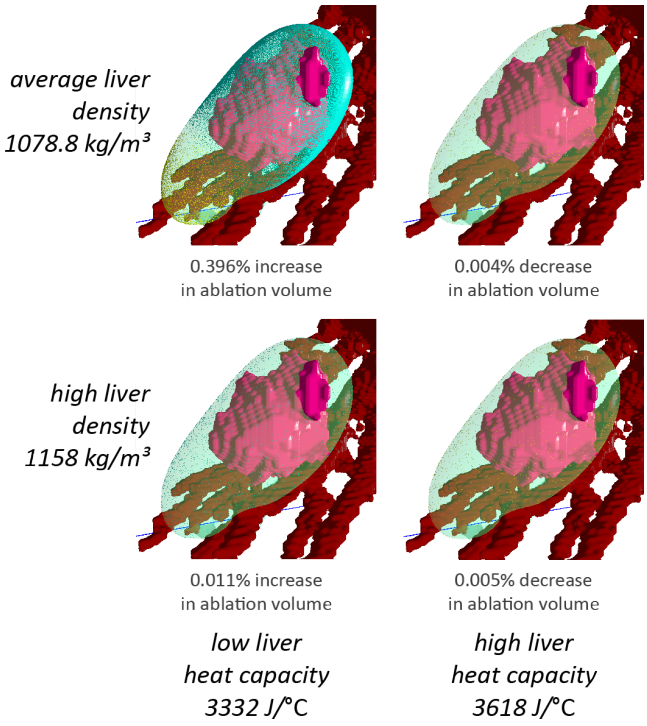

Figure 22: *Extracts of the 3D view illustrating the effect high density values have on the heat capacity's influence on the ablation volume. The change in volume is in relation to the ablation volume of the average property values (liver D = 1078.75 kg/m^3, liver HC = 3540.2 J/K)*

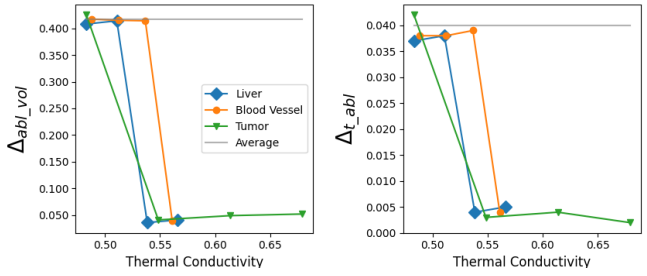

Figure 23: *The Δ_{abl_vol} and Δ_{t_abl} values of the dataset with different thermal conductivity values.*

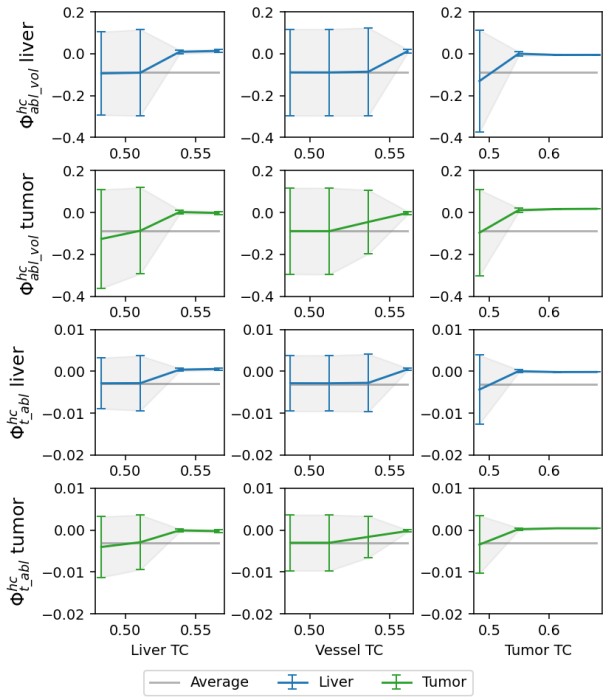

Figure 24: *The $\Phi^{hc}_{abl\_vol}$ and $\Phi^{hc}_{t\_abl}$ values and their standard deviation for the liver and tumor tissue with different density values for all tissue types.*

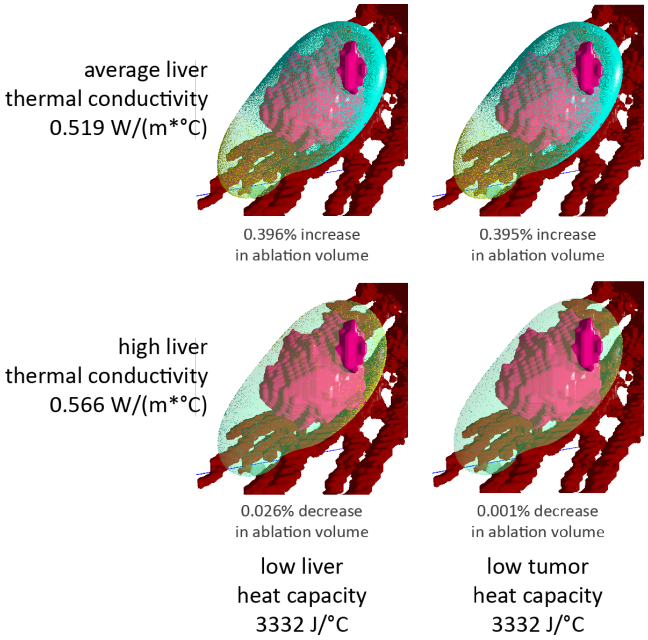

Figure 25: *Extracts of the 3D view illustrating the effect high thermal conductivity values have on the heat capacity's influence on the ablation volume. The change in volume is in relation to the ablation volume of the average property values (liver TC = 0.5191 $\frac{W}{m \cdot K}$, liver/tumor HC = 3540.2 J/K)*

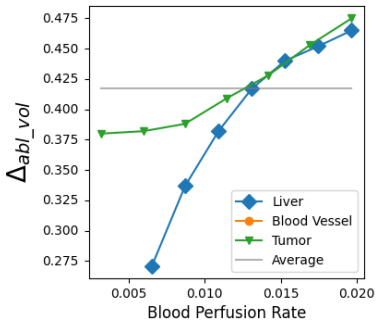

Figure 26: *The Δ_{abl_vol} value of the dataset with different blood perfusion values.*

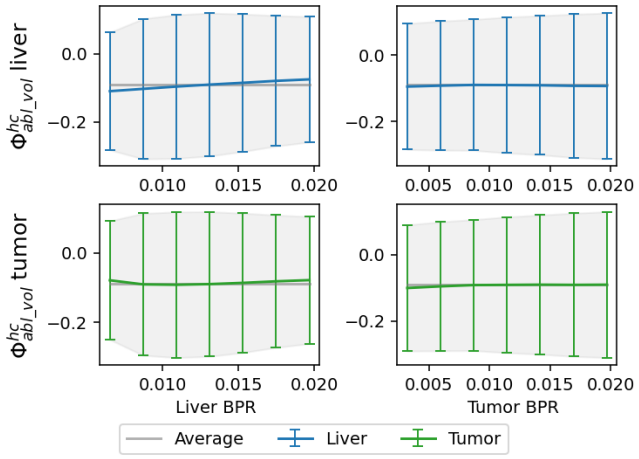

Figure 27: *The $\Phi^{hc}_{abl\_vol}$ values and their standard deviation for the liver and tumor with different blood perfusion values.*

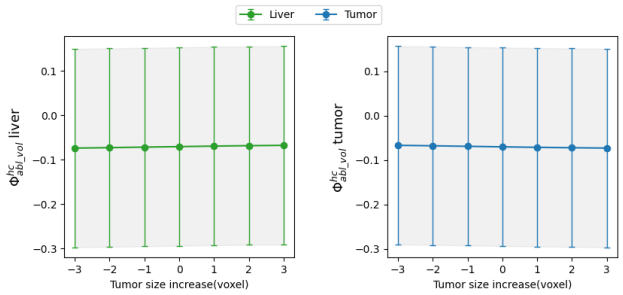

Figure 28: *The $\Phi^{hc}_{abl\_vol}$ values and their standard deviation for the liver and tumor tissue with modified tumor segmentations.*

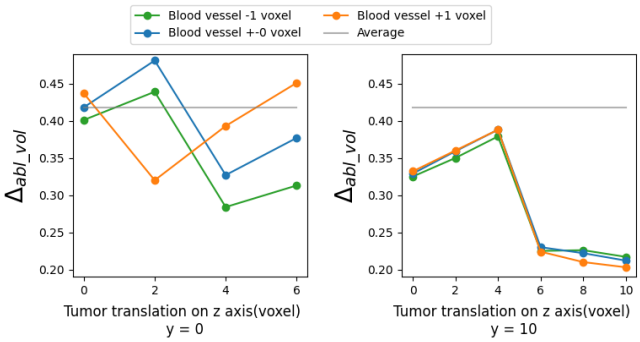

Figure 29: *The Δ_{abl_vol} and Δ_{t_abl} values of ensemble D.*

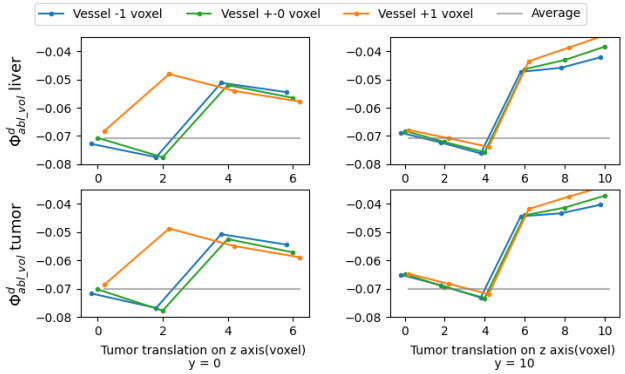

Figure 30: *The $\Phi^{hc}_{abl\_vol}$ values for the liver and tumor tissue with different different tumor segmentations and vessel sizes.*

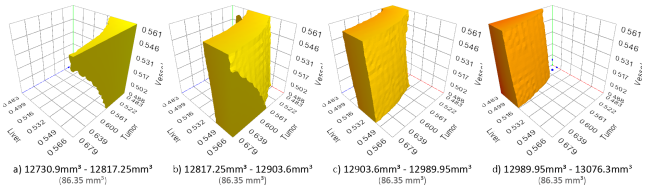

Figure 31: *Four surfaces of the ablation data plot visualizing the ablation volume size.*

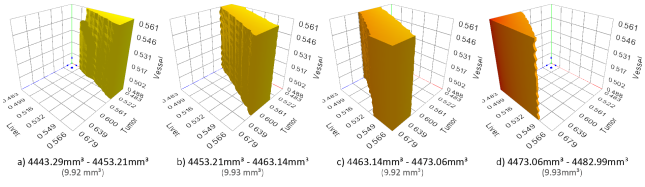

Figure 32: *Four surfaces of the ablation data plot visualizing the tumor ablation amount.*

near those blood vessel cells and a small overall increase of the ablation volume.

Increasing the tumor's thermal conductivity enlarges the ablation area around the tumor while reducing it everywhere else. An interesting part is the top of the ablation volume. There, the volume decreases in its size despite the close proximity of the tumor. Figure 35 highlights this behavior as it takes the ablation volume of the lowest tumor thermal conductivity as the intersect volume and shows the progression of the volume as the tissue property increases. One can observe how the reduction of the upper part of the ablation volume becomes bigger and bigger.

3.2. Ensemble B

In ensemble B, the density, heat capacity and blood perfusion rate were investigated as a secondary property.

For the density, higher values for the liver tissue slightly decrease the Δ_{abl_vol} and Δ_{t_abl} values of the dataset and thus reduce the impact the thermal conductivity has on the ablation area. Increasing the tumor's density results in the opposite behavior (see Figure 36).

The $\Phi^{tc}_{abl\_vol}$ and $\Phi^{tc}_{t\_abl}$ values of this dataset only show relatively small changes when changing the density of the tissues (see Figure 39). Higher liver density values seem to reduce the liver's impact on the ablation volume size while the impact of the other two tissue types slightly increases. The most notable change is the negative decrease of -0.152 of the liver's $\Phi^{tc}_{t\_abl}$ value when the tumor's density is at its highest value. However, these findings suggest, that the density's effect on the thermal conductivity is negligible.

In case of the heat capacity, the Δ_{abl_vol} and Δ_{t_abl} exhibit a similar behavior to the ones of the density dataset: Higher heat capacity values for the liver reduce the Δ values while higher values for the tumor lead to an increase (Figure 38). Just like for the density property, the $\Phi^{tc}_{abl\_vol}$ and $\Phi^{tc}_{t\_abl}$ values also show next to no change with varying heat capacity values.

In contrast to the density and heat capacity, the blood perfusion rate does lead to a significant change in the Δ and Φ values of the dataset. As shown in Figure 40, the Δ_{abl_vol} value is strongly influenced by the tumor's blood perfusion rate with a value of 1.770 for the lowest tumor perfusion and 3.535 for the highest. The liver's perfusion impacts the Δ_{abl_vol} the same way but on a much smaller scale.

Examining the Φ values in Figure 41 shows what causes these Δ_{abl_vol} value changes. Starting with the $\Phi^{tc}_{abl\_vol}$ value and the liver's blood perfusion values. Overall, the $\Phi^{tc}_{abl\_vol}$ values increase as the liver's blood perfusion rate grows. For the blood vessel and tumor, this positive increase in value leads to a reduction the respective tissue's impact on the ablation volume size since the $\Phi^{tc}_{abl\_vol}$ values go towards zero. The largest change is in the $\Phi^{tc}_{abl\_vol}$ value of the liver, which goes from -5.2 $\Phi^{tc}_{abl\_vol}$ to about -1.9 $\Phi^{tc}_{abl\_vol}$. This results in a decrease of the liver's impact on the ablation volume of over 60%. The $\Phi^{tc}_{abl\_vol}$ values of the other two tissue types are both similarly influenced by the liver's blood perfusion values with a maximum value change of 0.312 $\Phi^{tc}_{abl\_vol}$ for the tumor tissue and a change of 0.531 $\Phi^{tc}_{abl\_vol}$ for the vessel tissue.

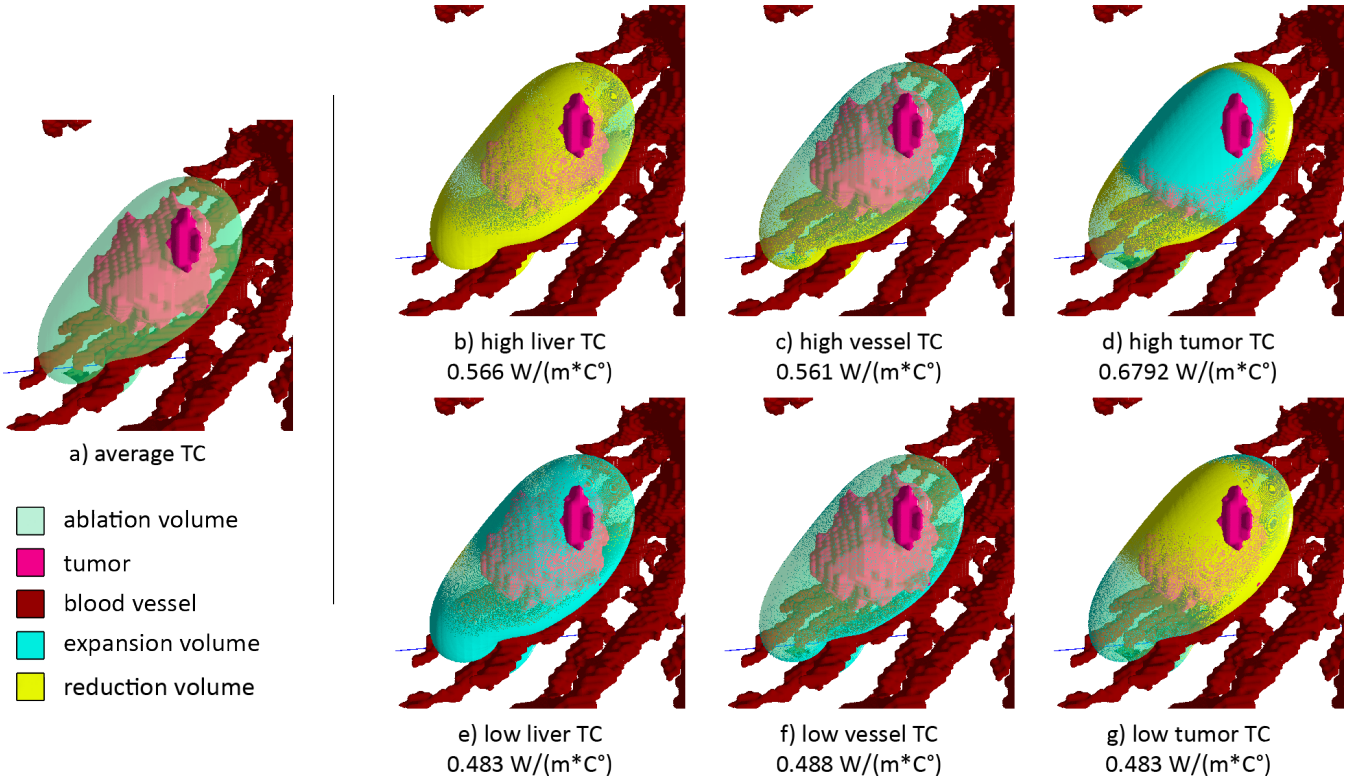

Figure 33: *Seven excerpts of the 3D view visualizing the change in ablation volume due to different thermal conductivity values.*

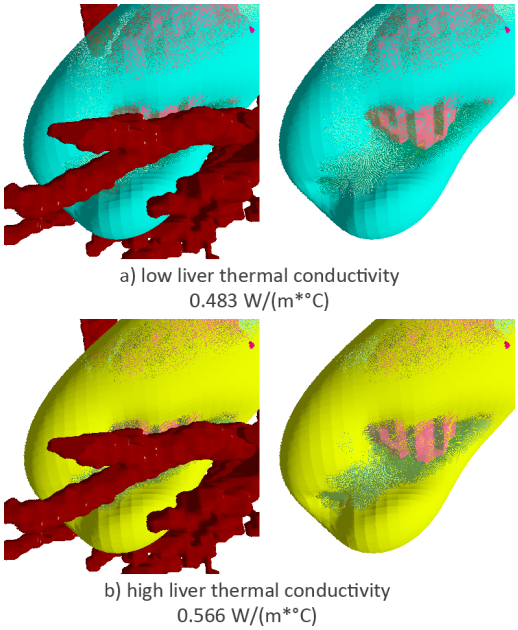

Figure 34: *Extracts of the 3D view with low and high liver thermal conductivity values, focused on a portion of the ablation volume which is close to blood vessels. The ablation volume of the average thermal conductivity values was used as the intersect volume.*

When the tumor's blood perfusion gets changed instead of the liver's, the $\Phi^{tc}_{abl\_vol}$ value of the blood vessel does not change at all. For the tumor values, an increasing tumor perfusion results in the same pattern as with the liver perfusion, but this time on a larger scale. With -0.380661 $\Phi^{tc}_{abl\_vol}$ as the lowest value for the tumor and 0.787403 $\Phi^{tc}_{abl\_vol}$ as the highest, the influence of the tumor's thermal conductivity on the ablation volume not only exhibits a sharp increase, but also changes from negative to positive. This means that the tumor's thermal conductivity negatively impacts the tumor ablation amount when its blood perfusion is low while it increases the ablation amount when the opposite is the case. The liver's $\Phi^{tc}_{abl\_vol}$ values behave differently when the tumor's blood perfusion is altered. Here, the $\Phi^{tc}_{abl\_vol}$ value of the liver negatively increases as the tumor's blood perfusion goes up with value of -1.74386 $\Phi^{tc}_{abl\_vol}$ for the lowest perfusion value and -2.96331 $\Phi^{tc}_{abl\_vol}$ for the highest.

Inspecting the ablation area of this dataset in the 3D view mostly shows no difference in the pattern of how the thermal conductivity affects the ablation area. The exception is the liver's thermal conductivity when the blood perfusion values for the tumor are lower than average. Figure 42 compares the effect of the thermal conductivity on the ablation volume with average and with low blood perfusion values for the tumor. As previously shown in Figure 33, the liver's thermal conductivity increases the parts where the tumor or the blood vessels get close to the edge of the ablation volume while also slightly increasing the rest of the ablation area. However when the blood perfusion values of the tumor are lower than average,

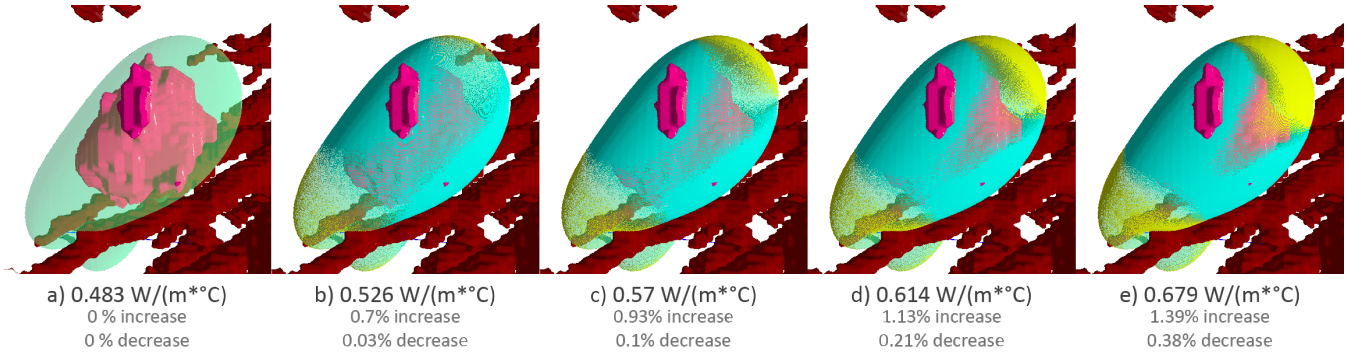

Figure 35: *Seven excerpts of the 3D view visualizing the change in ablation volume due to different thermal conductivity values.*

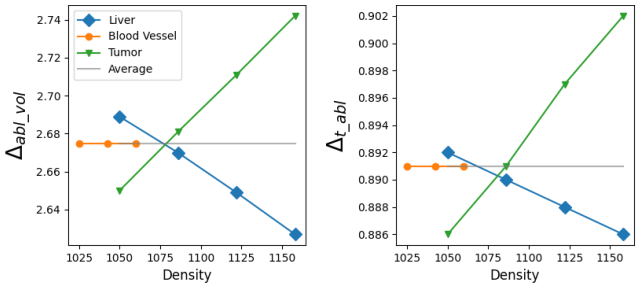

Figure 36: *The Δ_{abl_vol} and Δ_{t_abl} values of the dataset with different density values.*

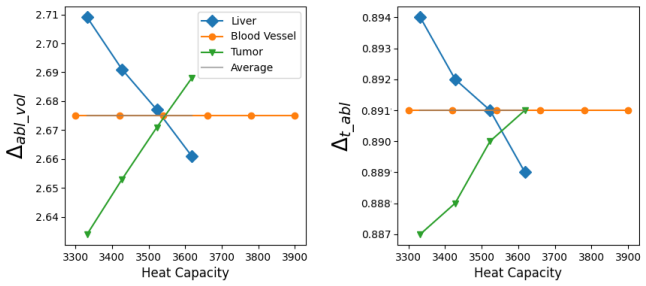

Figure 38: *The Δ_{abl_vol} and Δ_{t_abl} values of the dataset with different heat capacity values.*

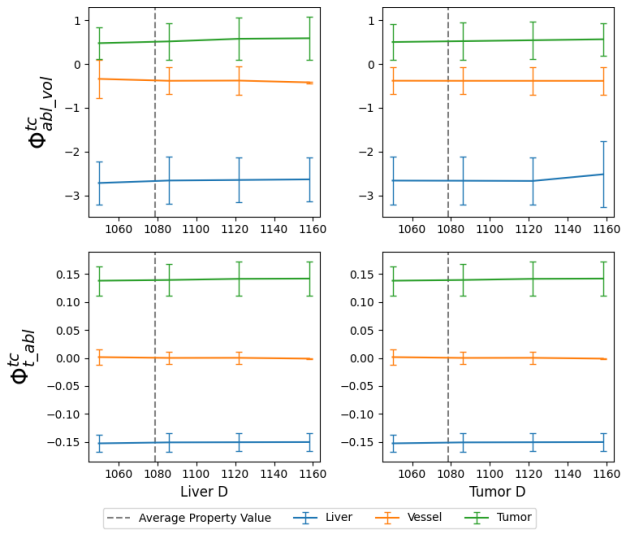

Figure 37: *The $\Phi^{tc}_{abl\_vol}$ and $\Phi^{tc}_{t\_abl}$ values and their standard deviation of the dataset with different density values.*

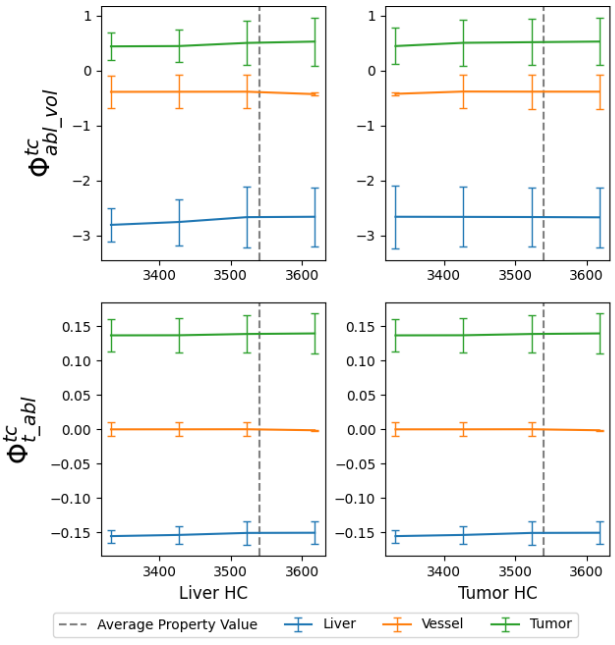

Figure 39: *The $\Phi^{tc}_{abl\_vol}$ and $\Phi^{tc}_{t\_abl}$ values of the dataset with different heat capacity values.*

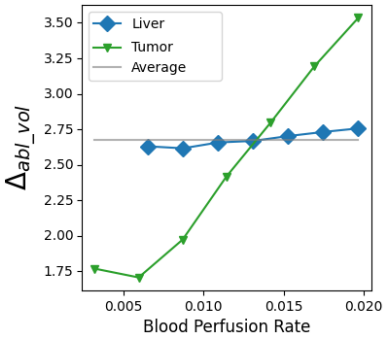

Figure 40: *The Δ_{abl_vol} and Δ_{t_abl} values of the dataset.*

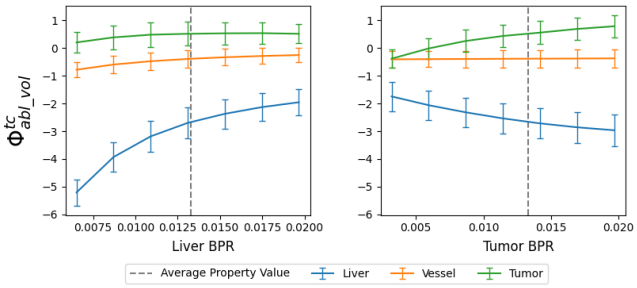

Figure 41: *The $\Phi^{tc}_{abl\_vol}$ and $\Phi^{tc}_{t\_abl}$ values of the dataset with different blood perfusion rate values.*

the volume only grows in the mentioned parts while it decreases slightly everywhere else. Below average thermal conductivity values lead to the opposite behavior.

3.3. Ensemble C

For ensemble C, Figure 43 displays the Δ_{abl_vol} values for the different tumor segmentations. The graph shows that the Δ_{abl_vol} value does not change for the smaller tumor sizes, while the enlargement of the tumor causes a sharp increase in its value. However, it must be noted that the thermal conductivity of the tumor is assumed to be up to 20% higher than the conductivity of the healthy liver tissue. This is most likely the explanation for the sharp increase of the Δ_{abl_vol} value as the tumor tissue takes up a larger part of the ablation volume and therefore its high thermal conductivity values affect the ablation volume size more. The stagnation of the Δ_{abl_vol} value for the smaller tumor sizes could indicate that the thermal conductivity of a volume below a certain size has no impact at all.

Figure 44 shows that the $\Phi^{tc}_{abl\_vol}$ value for the liver negatively increases as the tumor size gets bigger. In case of the $\Phi^{tc}_{abl\_vol}$ value, the tumor exhibits a special behavior: for a tumor size smaller than the original tumor, the thermal conductivity reduces the ablation volume on average, while it increases the volume for a larger tumor.

The inspection of the ablation volumes of the different tumor segmentations shows that the effects of the thermal conductivity of the liver and tumor on the ablation volume are strongly influenced by tumor size as shown in Figure 45. For both, the liver's and tumor's thermal conductivity the change in the ablation volume mainly affects the areas where the tumor is near the edges of the ablation volume. For a low liver thermal conductivity, the excerpts show that smaller tumors cause the ablation volume to partially decrease instead of consistently increasing as with the larger tumors. Higher thermal conductivity values result in the opposite effect, with a partial increase of the ablation volume with small tumors.

In the case of the tumor's thermal conductivity, the reduction in volume at low conductivity values and the increase in volume at high values becomes smaller as the tumor size decreases.

3.4. Ensemble D

For ensemble D, the Δ_{abl_vol} and Δ_{t_abl} values for the segmentations with a y-translation of 0 voxel increase as the ablation area gets closer to the blood vessels (see Figure 46). The segmentations with a smaller blood vessel size (-1 voxel) show a smaller increase than those with a larger blood vessel size (+1 voxel). For the other segmentations with a y-translation of 10 voxel the Δ_{abl_vol} value only slightly increases while the Δ_{t_abl} value displays an exponential growth when getting closer to the blood vessels.

Examination of the $\Phi^{tc}_{abl\_vol}$ values in Figure 47 shows that the liver and vessel thermal conductivity's impact on the ablation volume negatively increases when the tumor gets closer to the blood vessel cells. The $\Phi^{tc}_{abl\_vol}$ values of the tumor show no distinct pattern between the different segmentations. In case of the $\Phi^{tc}_{t\_abl}$ values, the segmentations with a y-translation of 0 voxel exhibit a similar behavior as the ones for the Δ_{abl_vol} values.

These findings suggest, that the impact of the liver's and vessel's thermal conductivity on the ablation volume and the tumor ablation amount increases as the ablation area gets closer to the blood vessels.

The inspection of the different segmentations in the 3D view shows no notable changes in the behavior of the ablation volume when the thermal conductivity is adjusted.

4. Relative Blood Perfusion Rate

4.1. Ensemble A

Relative blood perfusion rate has by far the most influence on the size of the ablation area and the tumor ablation amount. The difference between the maximum and minimum ablation volume for this tissue image amounts 13238 mm³ while the difference of the tumor ablation amount is 330.35 mm³ (see Table 12). These high values result in a Δ_{abl_vol} value of 103.661 and a Δ_{t_abl} value of 7.421.

For the analysis of this property only the liver and tumor tissue were inspected since the blood perfusion of the blood vessels is not supported by the TAS tool. It can be observed that the liver with a $\Phi^{bpr}_{abl\_vol}$ value of -77.329 has a way bigger impact on the ablation area than the tumor with a $\Phi^{bpr}_{abl\_vol}$ value of -17.761. However, both tissue types have almost the same $\Phi^{bpr}_{t\_abl}$ value which suggests, that the smaller the liver's perfusion is, the higher the ablation of the healthy non-tumorous tissue.

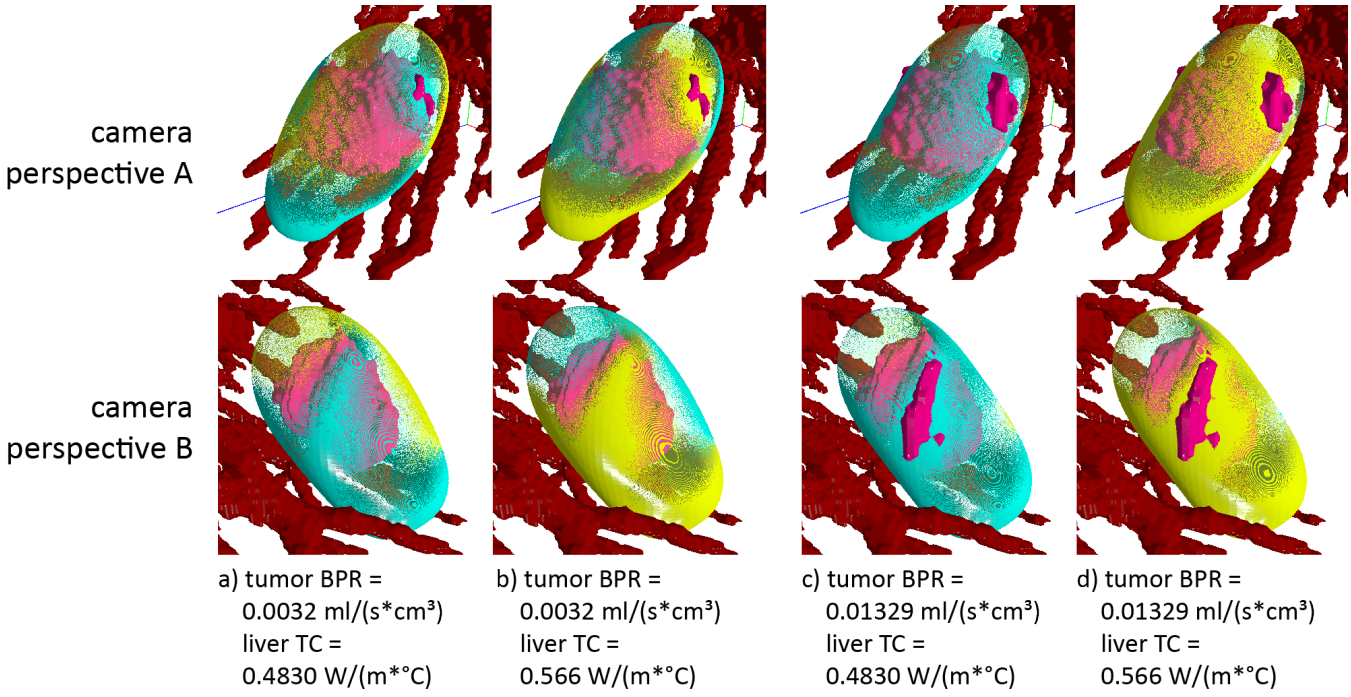

Figure 42: *Extracts of the 3D view displaying the ablation area changes with different tumor perfusion and liver thermal conductivity values.*

	Minimum	Maximum	Average	Max.-Min.	Δ
Ablation Volume	9309.85	22548.3	12770.9	13238.45	103.661
Tumor Ablation	4199.95	4530.3	4451.31	330.35	7.421

Table 12: *Ablation data measurements of the blood perfusion rate dataset of ensemble A.*

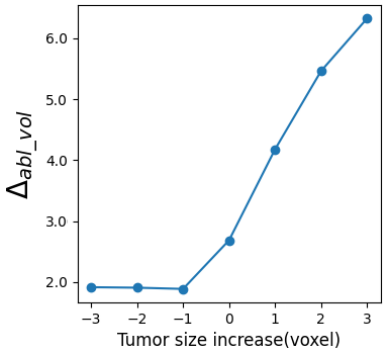

Figure 43: *The Δ_{abl_vol} values of the different tumor segmentations.*

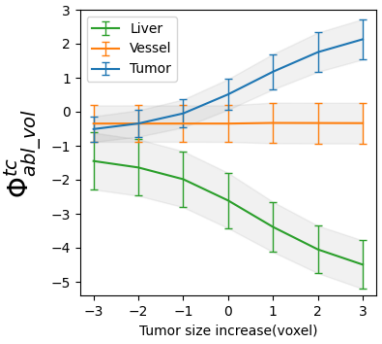

Figure 44: *The $\Phi^{tc}_{abl\_vol}$ values of the dataset with tumor segmentations.*

Another important aspect is the high standard deviation for both Φ^{bpr} values. The surfaces in Figure 49 show that the higher the blood perfusion of the liver, the lower its influence on the ablation volume size. This can be seen because the ablation volume intervals of the four surface are all the same, yet the coverage of the parameter space gets smaller. Therefore one unit of the blood perfusion rate has more impact on the ablation volume when the surface is relatively small.

For the tumor ablation amount, the opposite is the case: the impact of the liver's and tumor's blood perfusion on the tumor ablation increases with higher values (see Figure 50).

The inspection of the ablation volume in the 2D view and 3D view of TPAT visualizes the effect of different blood perfusion rate values on the ablation area. Within the extracts of Figure 51 the effects of low and high blood perfusion values for the liver and

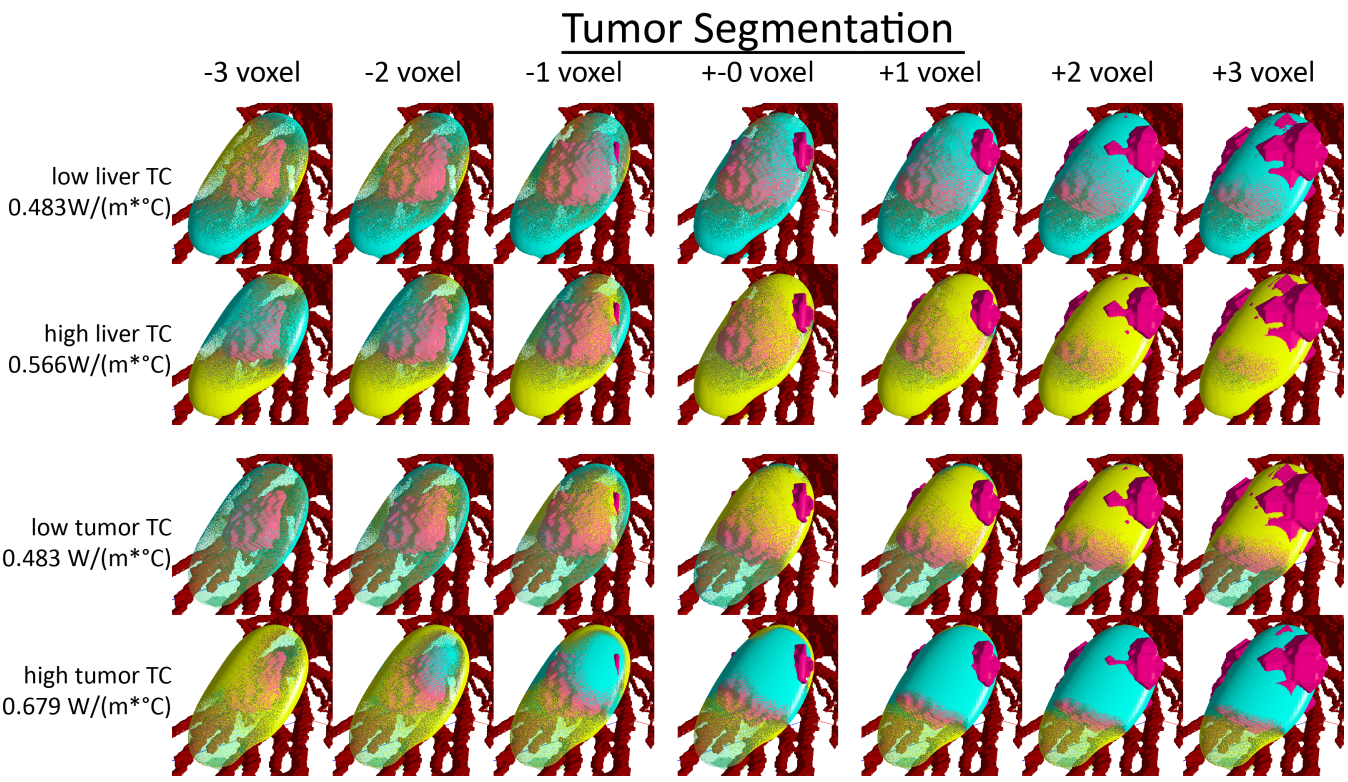

Figure 45: *The ablation volumes of the different tumor segmentations with high and low thermal conductivity values for the liver and tumor.*

	Φ^{bpr} liver	Stdev	Φ^{bpr} vessel	Stdev	Φ^{bpr} tumor	Stdev
Ablation Volume	-77.3292	41.4768	-	-	-17.761	3.32573
Tumor Ablation	-1.10389	0.741575	-	-	-1.09427	0.826016

Table 13: *The $\Phi^{bpr}_{abl\_vol}$ and $\Phi^{bpr}_{t\_abl}$ values of the dataset.*

tumor tissue can be seen. While the tumor's blood perfusion mostly affects the area around the tumor, the liver's leads to a more even expansion/reduction of the whole volume.

Closer inspection of the volume discloses that the impact of the blood perfusion rate greatly decreases in the proximity of blood vessels. Also, when the ablation volume is up close to a blood vessel, like in Figure 52, the blood perfusion rate of the liver has next to no influence on that portion of the ablation volume. Neither low nor high blood perfusion values seem to affect these parts.

4.2. Ensemble B

For the investigation of the influence of other tissue properties, the values for the density, heat capacity and thermal conductivity have been adjusted together with the blood perfusion rate. As for the density and the heat capacity, the Δ_{abl_vol} and Δ_{t_abl} values as well as the $\Phi^{bpr}_{abl\_vol}$ and $\Phi^{bpr}_{t\_abl}$ mostly stay the same for different property values. They both seem to not affect the blood perfusion's influence on the ablation volume at all.

Investigating the Δ_{abl_vol} values for the datasets where the thermal conductivity got modified displays a similar behavior for the liver and blood vessel tissue (see Figure 53). However, an increase of the tumor's thermal conductivity results in a considerable reduction of both Δ values. The graphs in Figure 54 disclose that an increase of the tumor's thermal conductivity negatively reduces the $\Phi^{bpr}_{t\_abl}$ values for the liver and tumor and the $\Phi^{bpr}_{abl\_vol}$ value for the tumor. Investigation of the ablation volume in the 3D view provides no new insights on this dataset.

4.3. Ensemble C

In ensemble C, the Δ_{abl_vol} value for the dataset increases as the tumor size increases. Just like for the thermal conductivity, this is due to the fact that the tumor's blood perfusion rate is assumed to possibly be much lower than the liver's perfusion rate. This results in a bigger maximum volume size when the tumor grows in size and therefore a higher Δ_{abl_vol} value. The graphs in Figure 56 show that the $\Phi^{bpr}_{abl\_vol}$ value for the tumor increases as its size grows while the liver's $\Phi^{bpr}_{abl\_vol}$ gets reduced. This is also simply the result of the tumor taking up more space and therefore having more influence

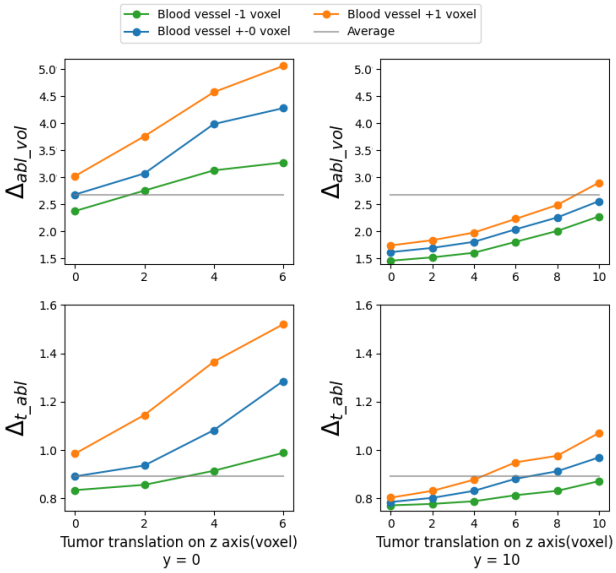

Figure 46: *The Δ_{abl_vol} and Δ_{t_abl} values of ensemble D.*

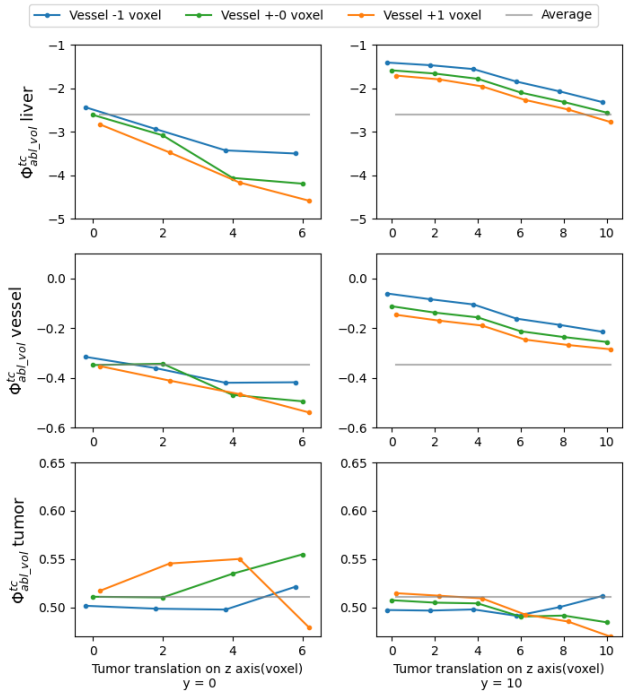

Figure 47: *The $\Phi^{tc}_{abl\_vol}$ values for the liver and tumor tissue with different tumor segmentations and vessel sizes.*

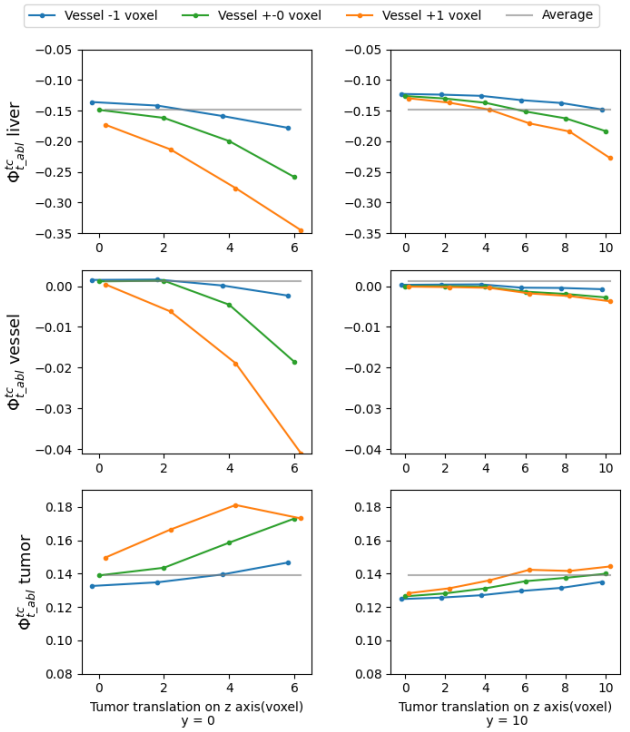

Figure 48: *The $\Phi^{tc}_{t\_abl}$ values for the liver and tumor tissue with different different tumor segmentations and vessel sizes.*

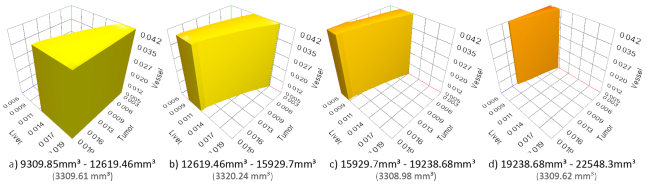

Figure 49: *Four surfaces of the with evenly sized ablation volume intervals.*

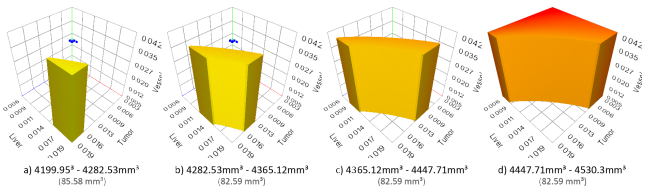

Figure 50: *Four surfaces with evenly sized tumor ablation amount intervals.*

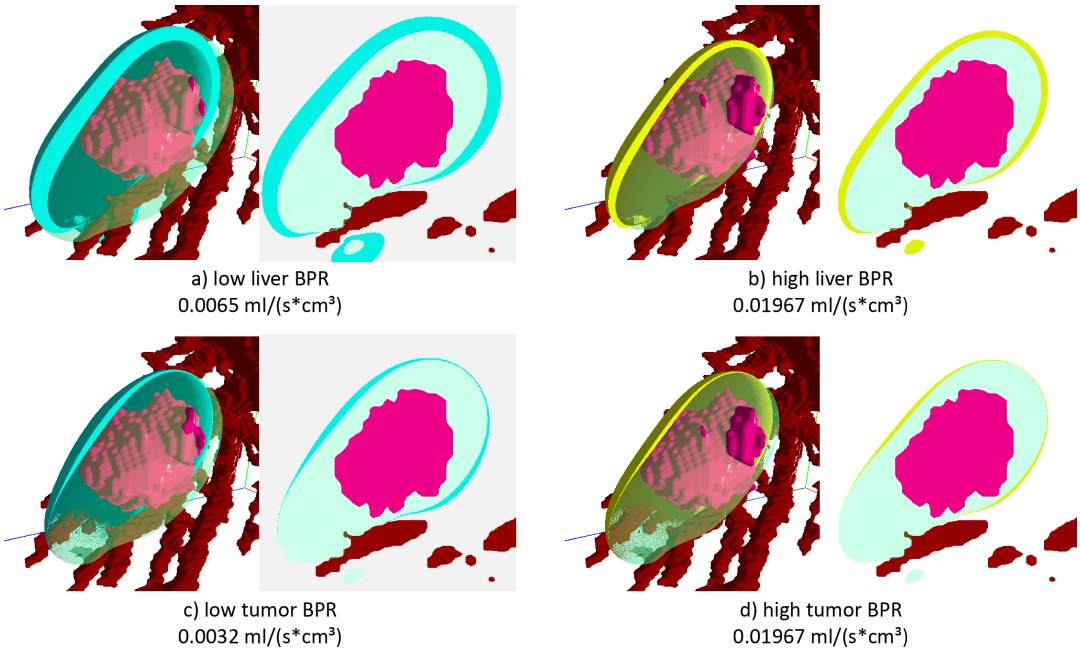

Figure 51: *Four excerpts of the 2D view and 3D view visualizing the change in ablation volume due to different blood perfusion rate values. The 3-dimensional volumes have been clipped to visualize the thickness of the ablation volume expansion/reduction.*

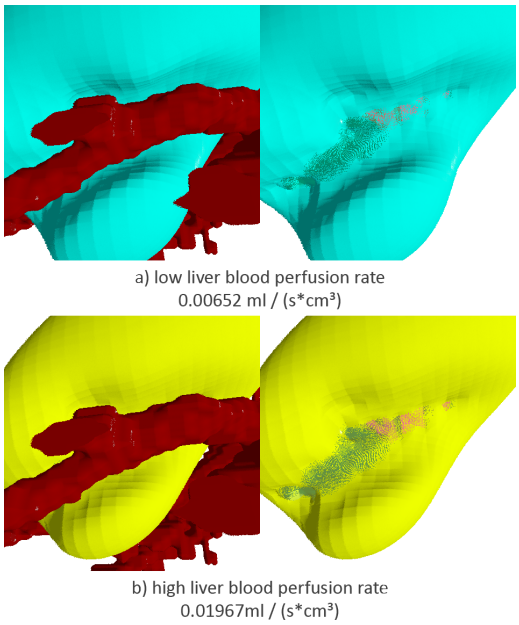

Figure 52: *Extracts of the 3D view with low and high liver blood perfusion rates, focused on a portion of the ablation volume which is close to blood vessels.*

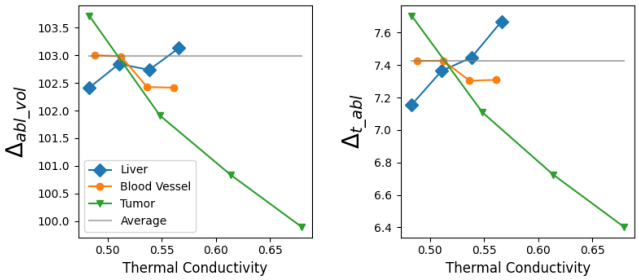

Figure 53: *The Δ_{abl_vol} and Δ_{t_abl} values of the dataset with different blood perfusion rates.*

on the ablation volume with its blood perfusion values. The extracts in Figure 57 display the increasing influence of the tumor's blood perfusion rate on the ablation volume when the tumor segmentation gets larger.

4.4. Ensemble D

The different tumor segmentations of ensemble D lead to a disparate behavior between the Δ_{abl_vol} and Δ_{t_abl} values. Figure 58 reveals a general decrease for the Δ_{abl_vol} values when the tumor is getting closer to the blood vessels whereby the segmentations with a y-translation of 10 show a sharper decrease than the others. For the Δ_{t_abl} values both segmentation groups show a growth in value whereas the segmentations with a y-translation of 0 show sharper increase.

This behavior is reflected in the Φ values in Figure 59: Segmen-

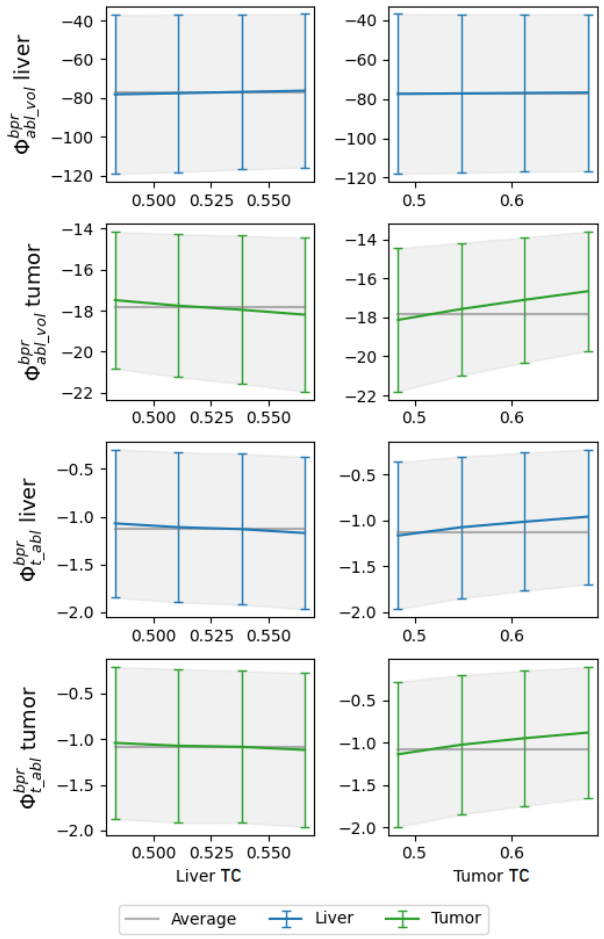

Figure 54: *The $\Phi^{bpr}_{abl\_vol}$ and $\Phi^{bpr}_{t\_abl}$ values of the dataset with different blood perfusion rates.*

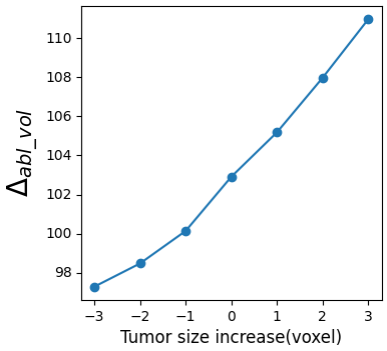

Figure 55: *The Δ_{abl_vol} values of the different tumor segmentations.*

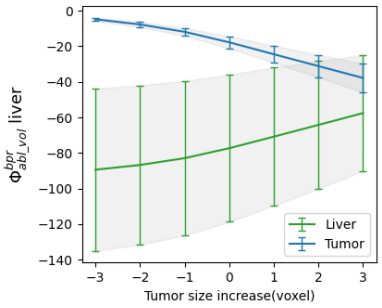

Figure 56: *The $\Phi^{bpr}_{abl\_vol}$ value of the dataset with different tumor segmentations.*

tations closer to the blood vessels reduce the influence of the liver's and tumor's blood perfusion on the ablation volume while their impact on the tumor ablation amount increases.

The inspection of the ablation volume in the 2D view and 3D view yields no new insights on the blood perfusion's impact on the ablation area. Nonetheless, Figure 60 visualizes the change in volume due to low liver blood perfusion values using the different segmentation's.

5. Other Tissue Properties

The generated datasets for the other 7 tissue properties displayed no change in their temperature fields with varying property values. For the optical and acoustic properties, who served as a control group, this was to be expected. However, the electric properties and the water ratio also did not affect the simulation output at all.

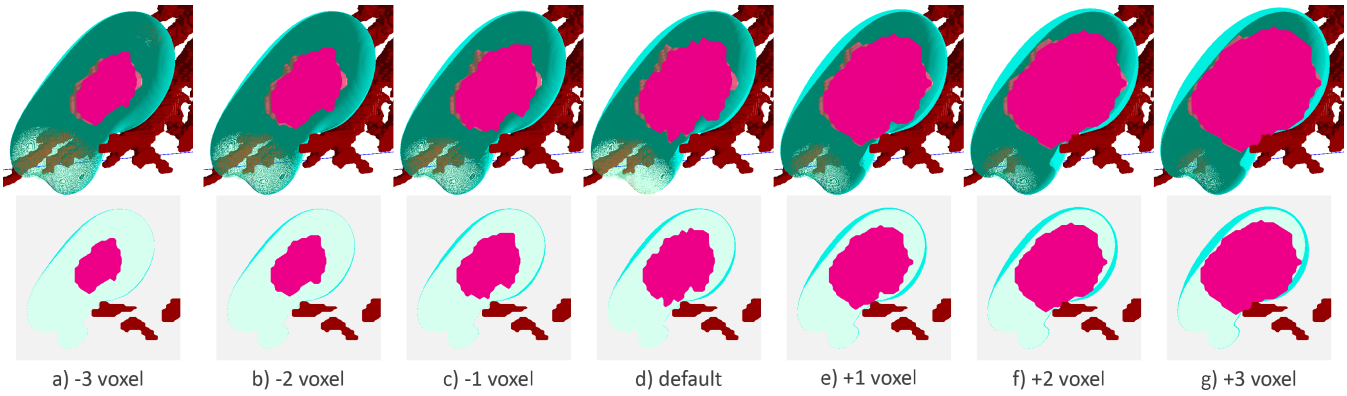

Figure 57: *Extracts of the 2D view and 3D view of the different tumor segmentations. The blue volume displays the difference between the ablation volume of low tumor blood perfusion values and the average values.*

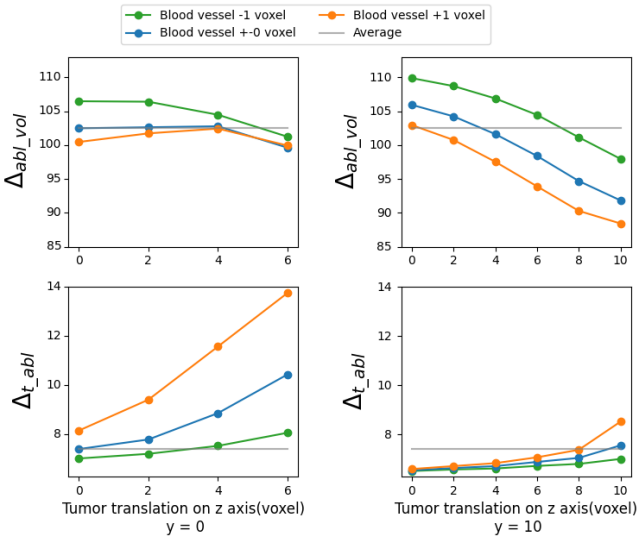

Figure 58: *The Δ_{abl_vol} and Δ_{t_abl} values of the dataset with different tumor segmentations.*

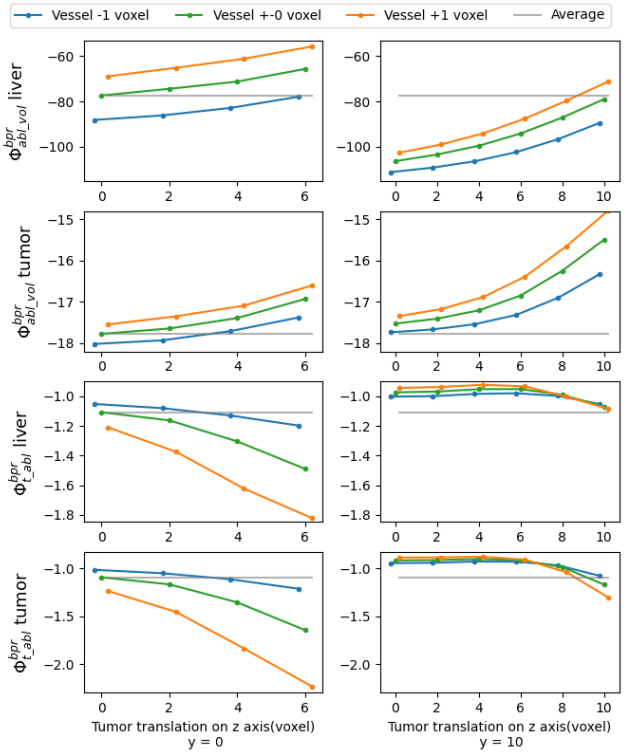

Figure 59: *The Φ_{abl_vol} and Φ_{t_abl} values of the dataset with different tumor segmentations.*

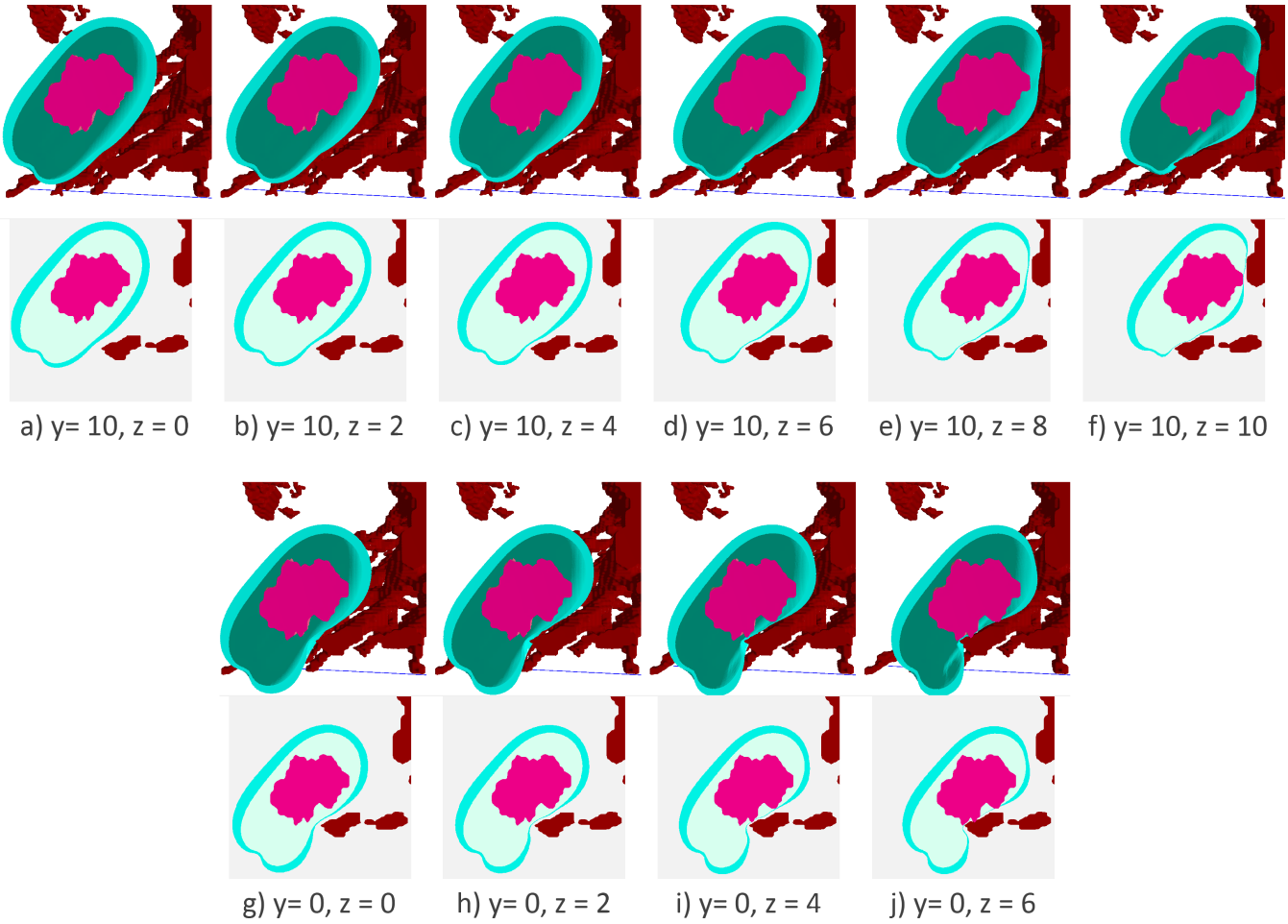

Figure 60: *Extracts of the 2D view and 3D view of the different tumor segmentations. The blue volume displays the difference between the ablation volume of low tumor blood perfusion values and the average values.*

Data set	Tissue	Interval	Step size	Data set size
Density	Liver	[1050,1158]	13.5	144
	Vessel	[1025,1060]	5.83	
	Tumor	[1050,1158]	13.5	
Heat capacity	Liver	[3332,3618]	47.66	200
	Vessel	[3300,3900]	66.66	
	Tumor	[3332,3618]	47.66	
Thermal conductivity	Liver	[0.483,0.566]	0.0166	216
	Vessel	[0.488,0.561]	0.0146	
	Tumor	[0.483,0.6792]	0.03924	
Rel. blood perfusion rate	Liver	[0.006519,0.019672]	0.000939	225
	Vessel	[0.023908,0.023908]	-	
	Tumor	[0.0032,0.019672]	0.001177	
Electric conductivity & Electric permittivity	Liver	[0.048542,0.055301]	0.001689	125
	Vessel	[0.851862,0.876469]	0.006152	
	Tumor	[0.024136,0.027496]	0.00084	
	Liver	[3620,2770]	-212.5	
	Vessel	[4570,4190]	-95	
	Tumor	[3620,2770]	-212.5	
Optical absorption	Liver	[1,250]	49.8	125
	Vessel	[1,250]	49.8	
	Tumor	[1,250]	49.8	
Optical scattering	Liver	[200,4500]	1075	125
	Vessel	[200,4500]	1075	
	Tumor	[200,4500]	1075	
Speed of sound	Liver	[1541.5,1611]	17.375	125
	Vessel	[1559.2,1590]	7.7	
	Tumor	[1541.5,1611]	17.375	
Acoustic absorption	Liver	[1,100]	24.75	125
	Vessel	[1,100]	24.75	
	Tumor	[1,100]	24.75	
Water ratio	Liver	[0.705,0.715]	0.0033	96
	Vessel	[0.782,0.813]	0.0062	
	Tumor	[0.705,0.715]	0.0033	

Table 14: *Tissue property values (parameter values) and ensemble sizes for ensemble A.*

Data set	Tissue	Interval	Step size
Density	Liver	[1050,1158]	36
	Vessel	[1025,1060]	17.5
	Tumor	[1050,1158]	36
Heat capacity	Liver	[3332,3618]	95.33
	Vessel	[3300,3900]	120
	Tumor	[3332,3618]	95.33
Thermal conductivity	Liver	[0.483,0.566]	0.02766
	Vessel	[0.488,0.561]	0.02433
	Tumor	[0.483,0.6792]	0.0654
Rel. blood perfusion rate	Liver	[0.006519,0.019672]	0.002192
	Vessel	[0.023908,0.023908]	-
	Tumor	[0.0032,0.019672]	0.002745
Electric conductivity & Electric permittivity	Liver	[0.048542,0.055301]	0.002253
	Vessel	[0.851862,0.876469]	0.008202
	Tumor	[0.024136,0.027496]	0.00112
	Liver	[3620,2770]	-283.33
	Vessel	[4570,4190]	-126.66
	Tumor	[3620,2770]	-283.33
Water ratio	Liver	[0.705,0.715]	0.005
	Vessel	[0.782,0.813]	0.01033
	Tumor	[0.705,0.715]	0.005

Table 15: *Tissue property values (parameter values) and the data set size for ensemble B.*